

Dense granular flow down an inclined plane: A comparison between the hard particle model and soft particle simulations

K. Anki Reddy and V. Kumaran

Department of Chemical Engineering, Indian Institute of Science, Bangalore 560 012, India

(Received 10 May 2010; accepted 22 September 2010; published online 10 November 2010)

The granular flow down an inclined plane is simulated using the discrete element (DE) technique to examine the extent to which the dynamics of an unconfined dense granular flow can be well described by a hard particle model. First, we examine the average coordination number for the particles in the flow down an inclined plane using the DE technique using the linear contact model with and without friction, and the Hertzian contact model with friction. The simulations show that the average coordination number decreases below 1 for values of the spring stiffness corresponding to real materials, such as sand and glass, even when the angle of inclination is only 1° larger than the angle of repose. Additional measures of correlations in the system, such as the fraction of particles with multibody contact, the force ratio (average ratio of the magnitudes of the largest and the second largest force on a particle), and the angle between the two largest forces on the particle, show no evidence of force chains or other correlated motions in the system. An analysis of the bond-orientational order parameter indicates that the flow is in the random state, as in event-driven (ED) simulations [V. Kumaran, *J. Fluid Mech.* **632**, 107 (2009); *J. Fluid Mech.* **632**, 145 (2009)]. The results of the two simulation techniques for the Bagnold coefficients (ratio of stress and square of the strain rate) and the granular temperature (mean square of the fluctuating velocity) are compared with the theory [V. Kumaran, *J. Fluid Mech.* **632**, 107 (2009); *J. Fluid Mech.* **632**, 145 (2009)] and are found to be in quantitative agreement. In addition, we also conduct a comparison of the collision frequency and the distribution of the precollisional relative velocities of particles in contact. The strong correlation effects exhibited by these two quantities in event-driven simulations [V. Kumaran, *J. Fluid Mech.* **632**, 145 (2009)] are also found in the DE simulations.

© 2010 American Institute of Physics. [doi:10.1063/1.3504660]

I. INTRODUCTION

Dense sheared granular flows are encountered in many applications, including geophysical applications such as avalanches as well as in industrial applications involving conveying of solids. In these flows, the energy required for “fluidizing” the system is provided by the mean shear and is not due to forcing at boundaries. In the modeling of dense granular flows, it is important to examine the range of densities and material properties for which the interaction between particles can be adequately represented as instantaneous collisions. Treating the interparticle interactions as instantaneous collisions results in several simplifications, the most important of which is the Bagnold form for the stress tensor where all components of the stress are proportional to the square of the shear rate. This would also facilitate the use of models based on kinetic theory calculations¹⁻⁹ to be applied for dense granular flows. However, there is as yet no consensus on whether dense granular flows can be modeled using an instantaneous collision model at all and in what parameter ranges. Partly, this is because a dense flow of hard particles involves two limiting processes. Multiple contacts are intuitively expected in the limit of volume fractions greater than about 50% in three dimensions, and the multiple contacts would occur more frequently when the coefficient of restitution is decreased. However, in the limit of hard particles (the elasticity modulus of materials, such as sand and glass, is of

the order of 100 GPa), the contact time between pairs of particles goes to zero, and one would expect the binary collision approximation to be valid provided the coefficient of restitution is $O(1)$. The balance between these two limiting process would determine the range of volume fractions and material properties for which a binary collision approximation is expected to be valid.

Large scale simulations¹⁰ of dense granular flows down an inclined plane have been able to provide a detailed description of the dynamics within the flow, which was not previously accessible in experiments. The simulations reveal several surprising features. It is found that the volume fraction in the bulk of the flow is a constant, independent of the total height and of conditions at the bottom boundary, and dependent only on the angle of inclination. All the components of the stress are found to be proportional to the square of the strain rate (Bagnold law); this relationship is a dimensional necessity if the only time scale in the flow is the inverse of the strain rate, and the period of particle interactions does not influence the flow dynamics (gravitational acceleration does not provide a material time scale since it provides a body force acting on the entire material and not a stress due to material deformation).

There have been some simulation studies¹¹⁻¹³ that have also indicated that the constitutive relations derived from the kinetic theory based on the binary collision approximation

are valid for these flows, while other studies^{14–17} suggested that long-range correlations are important and the kinetic theory cannot be applied for these flows. The simulations of Silbert *et al.*¹⁰ did show that the coordination number (number of particles in simultaneous contact with a particle) is larger than 1, indicating that multiple contacts dominate. However, the spring stiffness for interparticle interactions in that simulation was kept lower than that for real materials in order to increase the time step for the computations and decrease the computation time. Here, our focus is on the issue of the range of parameter values for which the flows of real materials can be well approximated by a hard particle model.

For a fluid of elastic particles, it is well known^{18,19} that the kinetic theory calculations are valid only in the dilute limit, and they become invalid at higher densities due to the effect of correlations. Correlations are incorporated by solving the ring-kinetic equation for the three-particle distribution function, and these correlations lead to the divergence of the viscosity in two dimensions [proportional to $\log(\dot{\gamma})$] and a contribution to the viscosity proportional to $\dot{\gamma}^{3/2}$ in three dimensions, where $\dot{\gamma}$ is the strain rate. The divergence of the transport coefficients is related to the long-time tails in the velocity autocorrelation function, which are due to the conserved nature of the transverse momentum fluctuations.²⁰ However, recent works, both theoretical^{21–23} and experimental,²⁴ have shown that the long-time tails in the velocity autocorrelation functions are not present in a sheared granular flow. This is because in contrast to a normal fluid, energy is dissipated in particle interactions in a granular flow, and so energy is not a conserved variable. Therefore, the kinetic theory for granular materials is valid for a larger range of volume fractions than that for molecular fluids.

Correlations are often interpreted as either dense clusters of particles or linear “force chains,” in which the stress transmission is concentrated in long chains of particles, which often extend from one boundary to the other, or as dense clusters of particles in correlated motion.^{16,17} While force chains are easily visualized in experiments on photoelastic disks,²⁵ they are more difficult to quantify, especially in three dimensional simulations or experiments. The significance of force chains could also depend on the conditions under which the material is deformed if the force chain is defined as a linear element with compressive stresses at both ends of the chain. If the material deformation is carried out under constant volume conditions and if the volume fraction is greater than the random close packing volume fraction, there will be multiple contacts between particles, which could be organized as chains of highly stressed particles spanning the sample. Alternatively, for flows with a free surface such as chute flows, it is difficult to envision force chains extending up to the surface since there is no compressive stress at the free surface. However, there could be force chains at a depth where the hydrostatic head provides the necessary compressive force on the particles, and these force chains could branch out and decrease in amplitude as the surface is approached.

Spatial correlations for the local collision frequency have been observed in hard particle simulations.²⁶ In two-dimensional silo simulations, particles within the flow hav-

ing the highest collision frequency were identified. The significant finding was that the particles with the highest collision frequency were formed linear structures, often system spanning in the cross-stream direction, which transmit most of the momentum. These structures experience slow relaxation, and the lifetime increases as the close packing volume fraction is approached. However, the authors were not able to extract a diverging length scale from the simulations. In a similar manner, Baran *et al.*²⁷ were also not successful in finding a diverging length scale in the simulations of the flow down an inclined plane. Experiments and simulations²⁴ show that the temporal velocity autocorrelation functions in a sheared granular flow decay faster than those in an elastic hard particle fluid at equilibrium.

In this regard, some recent results from hard particle event-driven (ED) simulations seems to suggest that all of the evidence is broadly consistent, provided it is interpreted carefully, as follows.^{28,29} In the rapid flow regime, the stress is proportional to the square of the strain rate (Bagnold scaling) on the basis of the dimensional analysis since the contact lifetime and the spring stiffness do not affect the dynamics. Soft particle simulations^{30–32} under constant volume conditions have shown that in the limit of high spring stiffness or low contact time, the flow exhibits Bagnold scaling for volume fractions of up to 0.58, but it seems to undergo a transition to the quasistatic regime at a volume fraction between 0.58 and 0.59. This was inferred as evidence that granular flows are always in the quasistatic regime even at volume fractions below the random close packing volume fraction of 0.64. This is in contrast to kinetic theories, which assumed that the kinetic regime could be extended to the random close packing volume fractions provided the particles were made stiff enough. However, recent ED simulations on hard particle systems^{28,29} have shown that the random close packing limit is lower in sheared inelastic fluids when compared to elastic fluids at equilibrium.

In hard particle systems,³³ the approach to random close packing is characterized by a diverging pair distribution function. In the empirical correlation proposed by Torquato,³³ the pair correlation function diverges proportional to $(\phi_c - \phi)^{-1}$, where $\phi_c = 0.64$ is the random close packing volume fraction for an elastic fluid at equilibrium. In a dynamical simulation, the divergence of the pair distribution function is measured by the divergence in the collision frequency since the collision frequency is proportional to the product of the pair distribution function and the square root of the temperature in the dense limit. It has commonly been assumed that the divergence of the pair distribution function in a sheared inelastic fluid also takes place at the volume fraction $\phi_c = 0.64$. However, some recent ED simulations indicate that the collision frequency in a sheared inelastic fluid diverges at a lower volume fraction, which is dependent on the coefficients of restitution.^{28,29} It should be noted that ED simulations suffer from the disadvantage of inelastic collapse very close to the random close packing limit, and numerical errors caused particle overlaps. However, this is different from the divergence of the collision frequency at the random close packing limit, which is a system property and not an artifact of the simulation, which occurs even for an elastic

fluid. The divergence of the collision frequency is inferred by plotting the inverse of the collision frequency as a function of the volume fraction and extending the curves to the horizontal axis. Data extrapolated in this manner^{28,29} show that the volume fraction for the divergence of the collision frequency for a sheared inelastic fluid is smaller than that for an elastic fluid. For the lowest coefficients of restitution in the range of 0.8–0.6, which were studied for rough particles, the collision frequency diverged at a random close packing volume fraction between 0.58 and 0.59. This implies that the seeming contradiction between soft particle simulations (which observed quasistatic scaling for volume fractions greater than about 0.59) and kinetic theory (where it was previously assumed that the random close packing volume fraction is 0.64) could be removed by replacing the random close packing volume fraction by the volume fraction for arrested dynamics ϕ_{ad} , which is defined as the volume fraction at which the collision frequency diverges in the sheared state. It should be noted that the distinction in ϕ_{ad} between a sheared and an unsheared system is different from the distinction between jamming and random close packing in collections of spheres^{34,35} since there is no applied shear in the latter case.

The above evidence is also consistent with large scale soft particle simulations of flows down an inclined plane,¹⁰ where the maximum volume fraction is observed to be about 0.59. In constant volume soft particle simulations, this is the maximum volume fraction at which the kinetic regime can exist in the limit of large spring stiffness, and above this volume fraction, the system is necessarily in the quasistatic regime where stress is transmitted by force chains. If force chains require compressive stresses at both ends, then force chains cannot exist in a flow with a free surface since there are no compressive forces on the free surface. Therefore, the system expands so that the volume fraction remains below the maximum limit for the kinetic transmission of stress. From the rapid flow perspective, the revised random close packing volume fraction in the presence of shear is in the range of 0.58–0.59, and so the flow down an inclined plane does not have a volume fraction greater than this. Therefore, the results of soft and hard particle simulations, constant volume and free surface simulations, as well as kinetic theory are all in agreement in this respect.

There is less agreement with respect to constant stress simulations, where the stress is kept as a constant and the volume fraction is varied. In this case, the distinction between the binary contact regime and the multibody contact regime has been made on the basis of the ratio of the average contact time in the simulation and the time period of a binary collision. Note that the time period of a binary collision is independent of the particle velocity in the linear contact model. Campbell³² reported that the system is in the multibody contact regime even when the overburden is of the order of one layer for 1 mm sand particles. This conclusion is based on an estimate of the spring constant based on the study of Bathurst and Rothenberg³⁶ discussed below. However, in the contact lifetime distribution for the flow down an inclined plane, Silbert *et al.*³⁷ found that the dynamics is dominated by the interactions with very short lifetimes. A

part of the difference may be because the simulations of Campbell³² are carried out with a constant stress, whereas those of Silbert *et al.*³⁷ and Brewster *et al.*³⁸ have a constant volume fraction and linear stress profile across the height of the flowing layer. More studies need to be done to resolve this contradiction.

Another interpretation of force chains emerges from contact-dynamics (CD) simulations,^{15,39} which are a combination of hard particle simulations (because they consider the resisting force to be infinite at contact) and molecular dynamics-type simulations (because the particles are advanced in constant time steps). Because the system evolution progresses in constant time steps and not in collision events, there could be multiple collisions in a given time step. In the case of multiple collisions, all the colliding particles are considered to be simultaneously in contact, and the impulses between the particles are determined on the basis of the collision laws. The solutions for the collision impulses for multiple particles in contact are not unique, however, and a procedure has to be devised to choose one of the possible solutions. In this case, multiple particles in simultaneous contact are considered to be force chains, and the stresses transmitted by these particles are considered to be “contact stresses,” in contrast to collisional stresses due to binary collisions.

There is a difference between the results of CD simulations and ED simulations with regard to the interpretation of multibody contacts. In two dimensions, ED simulations are able to access volume fractions up to about 0.76–0.8, depending on the coefficient of restitution (see Refs. 11 and 13, for example), and this simulation technique incorporates only binary collisions. At the same volume fraction, CD simulations (see Ref. 15, for example) indicate that the “static stress” (which includes multiple contacts) and the “collisional stress” (which is measured only over binary collisions) is larger than 1. The stress ratios in the abovementioned paper are plotted on a log scale, and so they become quite large. This implies that there are multibody contacts in two dimensions at volume fractions as low as 0.75. This indicates a clear difference between hard particle and contact-dynamics simulations with regard to force chains, and it would be worthwhile to examine whether the time resolution alters the multibody contact network in contact-dynamics simulations.

The simulations of Lois *et al.*^{40–42} were all restricted to two dimensions. In their studies, it was observed that the volume fraction, temperature, and strain rate profiles obtained in the CD simulations were similar to those in discrete element (DE) simulations. However, Lois *et al.*¹⁵ concluded that kinetic theory does not apply to dense flows due to enduring contacts in the CD simulations. In particular, they have compared the “kinetic” and “static” stresses to show that multibody contacts are important at high densities. For dense shear flows, Lois *et al.*⁴⁰ formulated a shear transformation zone theory, following an earlier work on the deformation of amorphous solids under shear.^{43,44} For this, they introduced additional state variables and transition probabilities for the local rearrangements in the flow. These transition probabilities are related to the granular temperature and the

ratio of the shear and normal stresses, and these relations involve material constants. These constants were fitted using simulation results for the variation of (σ/p) with $(\dot{\gamma}d/\sqrt{T})$ for a steady shear flow in the absence of gravity using Lees–Edwards boundary conditions. Here, σ and p are the shear stress and pressure, $\dot{\gamma}$ is the strain rate, T is the granular temperature, and d is the particle diameter. The authors found that the dependence of (σ/p) on $(\dot{\gamma}d/\sqrt{T})$ is the same for a homogeneous shear flow and for the flow down an inclined plane if the same particle interaction law is used.

The work of Lois *et al.*¹⁵ was also one of the motivations for modifications of the inelastic dissipation rate by Jenkins^{16,17} to account for the correlated motions in a dense granular flow. While these modifications do provide better agreement between kinetic theory and simulations, the presence of correlations should also be independently verifiable in soft particle simulations since all microscopic variables are accessible in these simulations. Detailed studies²⁷ of the velocity autocorrelation function in dense flows using DE simulations have not detected any long-range velocity correlations. There is an unresolved issue that multibody contacts are present in CD simulations, while they are absent in ED simulations at the same area fraction in two dimensions.

In the inclined plane simulations,¹⁰ it is also observed that the stress is accurately described by Bagnold law for variations in the spring constant over many orders of magnitude. In fact, the Bagnold law appears to be applicable even when the particles are in the multibody contact regime, and the magnitudes of the stresses do not change very much as the spring stiffness is increased and the system transitions from a multibody contact regime to the binary collision regime. This is a puzzle that has not been satisfactorily resolved. One possible explanation is that even though there are multiple contacts, there is one dominant force on a particle. This is in contrast to the quasistatic regime where the particle is simultaneously acted on by forces from many neighbors, which are roughly of the same magnitude. This explanation was explored by Reddy and Kumaran,¹² who found that the average ratio of the magnitude of the second largest to the largest force is quite small even in the multibody contact regime. A related explanation (Ref. 37) is that particle motion is dominated by short-lived contacts for large spring stiffnesses, although the appearance of long-lived contacts was accompanied by the breakdown of Bagnold rheology as the stiffness of interparticle contacts was decreased. Further work needs to be done to resolve this issue.

One question is whether the constitutive relations based on the kinetic theory can reproduce all the qualitative features of a dense granular flow. This is slightly different from the issue of whether the flow is actually in the binary contact regime because simulations of the flow down an inclined plane (Refs. 37 and 12) have consistently shown that there is very little variation in the stress components for a given flow as the spring stiffness of interparticle contacts is changed for a given angle of inclination. The stress components vary by only 10%–20% when the spring stiffness changes by three to four orders of magnitude, and the dynamics transitions from the multibody contact to the binary collision regime. Therefore, it is necessary to examine two questions separately: the

first being whether the flow can be modeled using constitutive relations based on the kinetic theory and the second whether the flow is actually in the binary contact regime.

For the flow down an inclined plane, it is now clear that all the qualitative features can be reproduced using constitutive relations obtained from the Chapman–Enskog procedure.^{45,46} In addition, it has been known that the stresses in the flowing granular materials are fairly well predicted by constitutive relations from the kinetic theory, but the energy dissipation rate due to inelastic collisions are consistently overpredicted.¹¹ The quantitative differences, primarily in the energy dissipation rate, have been attributed to correlations not captured by the binary contact model in earlier studies.^{16,17} More recent works^{28,29} on the comparison between theory and hard particle simulations have shown that the quantitative difference in the dissipation rate could be explained by a change in the form of the distribution of precollisional relative velocities between colliding particles. It should be noted that in a dense flow, the stress transmission and energy dissipation occur primarily due to collisions, and the collisional stress and dissipation rate depend on the distribution of precollisional relative velocity between pairs of colliding particles.

It should be noted that the hard particle model, with which we compare our simulations results, is different from the kinetic theory because velocity correlations between colliding particles are included in the form of a modified relative velocity distribution at collision. The Chapman–Enskog procedure assumes that the two-particle velocity distribution function is the product of the single-particle distributions and the pair distribution function at contact. It is known that constitutive relations obtained using the Chapman–Enskog procedure do predict qualitatively, but not quantitatively, the stresses and dissipation rate in a dense granular flow.⁴⁶ Hard particle simulations²⁹ indicate that this approximation is not valid in a dense flow, and the distribution of the relative velocities undergoes a transition from a Gaussian distribution to an exponential distribution as the coefficient of restitution is decreased. If the correct form of the relative velocity distribution is incorporated in the theory, it is possible to quantitatively predict the stresses and the dissipation rate. Therefore, it is clear that quantitative agreement between simulations and hard particle simulations can be obtained if the effect of correlations on the relative velocity distribution of colliding particles is incorporated. It should be emphasized that the “hard particle model” used here for comparison is not the standard kinetic theory, but does include the effect of correlations.

Recent studies of Silbert *et al.*³⁷ and Brewster *et al.*³⁸ on the lifetime of contacts between particles seem to suggest that particle interactions are dominated by short-lived contacts, and the study of Reddy and Kumaran¹² indicated that the coordination number is smaller than 1 when the spring constant suitable for real materials, such as sand and glass, are used in the simulations. In contrast, the studies of Campbell^{31,32,47} report that the flows of real materials are always in the multiple contact regime and conclude that the binary collision approximation is not valid for most situations of practical interest. As discussed above, one source of

disagreement is resolved by recognizing that the volume fraction for arrested dynamics for a sheared inelastic fluid is smaller than the random close packing volume fraction for an elastic fluid. In addition, the force chains observed in controlled volume experiments are not likely to be seen in flows with a free surface due to the lack of a compressive stress at the free surface. The second source of disagreement is the differences in the estimates for the spring stiffness for the interaction between two particles.

The two force-displacement contact laws that are widely used in simulations for elastic particles are the linear (Hookean) and the Hertzian contact laws, where the normal restoring forces are $f=k_n\delta$ and $f=k'_n\delta^{3/2}$, respectively, where δ is the linear deformation of two contacting particles perpendicular to the surfaces of contact. For inelastic particles, these relations are modified by including viscous damping terms, and similar relations can be written for the tangential force at contact as a function of the tangential displacement. The Hertzian contact law accounts for the increase in the area of contact between two smooth particles as the deformation increases and is therefore better suited for contacts between smooth particles. However, the linear contact law has a constant binary collision lifetime, independent of the approach velocities, and is consequently more widely used. In order to perform realistic simulations, it is necessary to determine the constants k_n and k'_n from the material properties of the grains.

If we assume that the spring constant depends only on the elasticity modulus E and the particle diameter d , then by dimensional analysis, the spring stiffness for the linear contact law k_n is proportional to (Ed) , while that for the Hertzian contact law, k'_n is proportional to $(Ed^{1/2})$. The estimate (Ed) has been used by Silbert *et al.*¹⁰ and Reddy and Kumaran¹² for the linear spring constant in simulations. For the Hertzian contact model, an exact calculation by Mindlin and Deresiewicz⁴⁸ shows that $k'_n \propto Ed^{1/2}$, in agreement with the estimate based on the dimensional analysis. Since most materials (such as sand and glass) have an elasticity modulus of the order of 10^{11} N/m², this results in the spring stiffness of the order of 10^9 N/m for 100 μ m particles for the linear model and a spring stiffness of the order of 10^{11} N/m^{3/2} for the Hertzian model. The estimates of the dimensionless spring stiffness for linear and Hertzian contacts $[k_n/(mg/d)]$ and $[k'_n/(mg/d^{3/2})]$, which are both proportional to (Ed^2/mg) , are given in Table I. It should be noted that at constant mass density and Young's modulus, the scaled spring stiffness are proportional to $(1/d)$.

The estimate of Campbell^{31,32,47} has been based on the measurements of sound speed of the order of 100 m/s in loose sand,³⁶ which provides an elasticity modulus of the order of 2×10^7 N/m², and a spring constant of the order of 10^3 – 10^4 N/m for particles with diameter between 100 μ m and 1 mm. This estimate has led Campbell^{31,47} to conclude that flows of real materials are always in the multiple contact regimes. This procedure is not in agreement with the Mindlin–Deresiewicz calculation for the spring constant in the Hertzian contact law, which is based on the compression modulus of the sand particle itself and not the compression modulus of a loose assembly of sand grains.

TABLE I. The Young's modulus Y , Poisson ratio ν , mass density ρ , the dimensionless number (Ed^2/mg) , which is the estimate for both the dimensionless linear spring stiffness $[k_n/(mg/d)]$, as well as the dimensionless Hertzian spring stiffness $[k'_n/(mg/d^{3/2})]$ for spheres with a diameter of 100 μ m some common materials.

Material	Y (10^{-9} Pa)	ν	ρ (10^{-3} kg/m ³)	$(Ed^2/mg) \times 10^{-10}$
Iron/steel ^a	190–210	0.27–0.30	7.83	4.63–5.13
Copper ^a	130	0.33	8.96	2.77
Aluminum ^a	70	0.33	2.70	4.94
Sand ^b	90–125	0.2–0.45	2.50	6.87–9.55
Glass ^c	50–90	0.18–0.3	2.60	3.67–6.61

^aReference 49.

^bReference 50.

^cReference 51.

Experimental results have more recently become available, which directly measure the stiffness of contacts between particles.^{50,52} In these experiments, two individual grains of sand were mounted on pins with a diameter of 2 mm and pressed against each other. The normal displacement and the normal force were simultaneously measured, and the particle contact stiffness was inferred from these. The radius of curvature of the surfaces at contact was in the range 0.05–8.2 mm. There are several surprising results from these experiments. One of these is that for several different types of sand, the force law at small forces is linear instead of Hertzian. This is because in the initial stages, the deformation is due to the compression of asperities on the surface, instead of the compression of two smooth surfaces in which the contact area increases with time. The spring constant in the Hertzian contact regime is well predicted by the Mindlin–Deresiewicz theory, and the numerical results are about 20% lower than the value that would be obtained if the elasticity modulus of the material is inserted into the Mindlin–Deresiewicz relation. The spring constant for the linear contact law at low forces is in the range of 0.2 – 2×10^6 N/m for a large class of materials. This spring constant is an order of magnitude smaller than the estimates of Reddy and Kumaran¹² for particles of 100 μ m in diameter, but is about two to three orders of magnitude larger than that obtained using the speed of sound through loose sand. In our calculations, we use the linear spring constant of $k_n=0.5 \times 10^6$ N/m as a reference value based on the experiments of Cole and Peters.^{50,52} For particles with a mass density of 2500 kg/m³, this results in a dimensionless spring stiffness $[k_n/(mg/d)]$ in the range of 3.82×10^9 – 3.82×10^7 for particles with diameter in the range of 100 μ m–1 mm. In this case, it should be noted the scaled spring constant decreases proportional to $(1/d^2)$ as the diameter is increased at fixed k_n and mass density. This is in contrast to the decrease proportional to d^{-1} when Young's modulus and mass density are fixed.

For the Hertzian contact model, as discussed earlier, experiments show that k'_n scales as $Ed^{1/2}$. A lower bound on the elasticity modulus for materials, such as sand and glass, is $E \sim 0.5 \times 10^{11}$ N/m² (see Table I), and if we assume a mass density of 2500 kg/m³, the nondimensional spring stiffness

$[k_n'/(mg/d^{3/2})]$ varies in the range of 3.82×10^{10} – 3.82×10^9 for particles with diameter in the range of $100 \mu\text{m}$ – 1 mm . In this case, the scaled spring stiffness decreases proportional to $(1/d)$ as the particle diameter d is increased at constant elasticity modulus and mass density. For both linear and Hertzian contact models, it is difficult to obtain results for scaled spring stiffness greater than about 10^8 due to computational limitations. In the present analysis, the trends in the structure and the dynamics are examined for scaled spring stiffness in the range of 2×10^5 – 2×10^8 .

The effect of the stiffness of particle contacts on the particle interactions in the flow down an inclined plane is examined by calculating the coordination number, which is the average number of particles that are in simultaneous contact with a particle. In addition, the fraction of particles that overlap with $1, 2, 3, \dots$ other particles is also calculated in order to examine the conditions under which the system is in a binary/multibody contact regime. The particle interaction models analyzed are the linear contact model with and without friction, as well as the Hertzian contact model with friction.

An important measure of ordering in the flow is the icosahedral order parameter Q_6 because it gives us information about the state of order in the flow.⁵³ For a fluid of elastic hard particles at equilibrium, the order parameter Q_6 is 0 when the volume fraction is below 0.49. However, at 0.49, there is spontaneous crystallization to a face centered cubic (fcc) packing, and Q_6 becomes nonzero. This implies that kinetic theories based on dense gases cannot be used for a volume fraction higher than 0.49 because the system is in a crystalline state with a definite lattice symmetry. Since dense granular flows mostly have a volume fraction higher than 0.49, this means that the kinetic theories based on an isotropic pair distribution function are not valid. This leads Jenkins,¹⁷ for example, to employ a different set of constitutive relations for volume fractions greater than 0.49.

Recently, in simulations of sheared granular flows, it has been found using ED simulations that there is no spontaneous crystallization transition, and the system is in the random state even up to a volume fraction of 0.6.^{28,29} Shear spontaneously breaks the ordering in the system. If hard particle theories based on a random state are to be applicable to the flow down an inclined plane, then it is important to check that the relative arrangement of particles is, in fact, random in the DE simulations, and there is no fcc or hexagonal closed packed (hcp) ordering in the system. That is why the parameter Q_6 is important to verify that the state of order in the DE and ED simulations is the same.

An attempt is also made to analyze the effect of correlations in the flow. Previous simulation studies²⁷ have shown that the spatial correlations in the velocities are insignificant. Our simulation results lead to the same conclusions, and so we do not report these here. Previous experimental²⁴ and simulation²⁸ studies have also shown that the time decay of the velocity autocorrelation function is much faster than that in an elastic fluid at equilibrium. Here, we examine the correlations in the forces acting on a particle using two measures, the “force ratio” and the “force angle,” which are discussed in detail later.

There are two important phenomena that significantly influence the dynamics in the shear flow of hard inelastic particles.^{28,29} The first, discussed above, is the divergence of the collision frequency at the volume fraction for arrested dynamics ϕ_{ad} , which is lower than the random close packing volume fraction for elastic particles at equilibrium. The second is the change in the form of the precollisional relative velocity of colliding particles from the Gaussian relative velocity distribution for elastic particles to an exponential distribution for inelastic particles with normal coefficient of restitution $e_n < 0.8$. Both of these effects are examined in DE simulations of particles with finite spring stiffness. It is important to note that discrete collisions cannot be defined in the multibody contact regime where the coordination number is larger than 1. Therefore, the collision frequency and the relative velocity distribution are examined only for the largest spring stiffness $[k_n'/(mg/d)] = 2 \times 10^8$ used in the present study.

The results for the Bagnold coefficients from the DE simulations are compared with the results of event-driven simulations.^{28,29} In order to make a quantitative comparison, we use a linear spring-dashpot model with no friction in the DE simulations. The spring constant k_n in the direction normal to the surfaces of contact is varied in the range of 2×10^5 – 2×10^8 , while the damping constant γ_n is adjusted to obtain the same coefficient of restitution for two-body contacts as that used in the ED simulations. The damping constant in the direction tangential to the surfaces at contact γ_t is set equal to zero so that there is no dissipation due to displacement in the tangential direction. For a linear contact model with no friction, we obtain a steady flow only when the normal coefficient of restitution is less than 0.9, and so we report results for normal coefficients of restitution in the range of 0.6–0.8.

As formulated above, the DE model exactly corresponds to the rough particle model with $e_t = 1$, where the relative tangential velocity is reversed in a collision. Since the contact model in the DE simulations exactly corresponds to the collision model in the event-driven hard particle simulations, it is possible to make a quantitative comparison of the Bagnold coefficients obtained by the two techniques. In addition, we also compare the simulations with the predictions of the theory,²⁹ which included the divergence of the collision frequency at $\phi_{ad} < \phi_c$ under shear and the modification of the relative velocity distribution due to correlations.

In an inclined plane flow, the volume fraction is a constant and the stress satisfies the Bagnold law in the bulk of the flow, where the distance from the boundaries is large compared to the “conduction length.”¹⁰ This is because the conduction term in the energy balance equation is small compared to the production of energy due to mean shear and the dissipation due to inelastic collisions in the bulk of the flow⁴⁶ and from the momentum balance equations (1) and (2) below. However, near the top and bottom boundaries, there are “conduction boundary layers” of thickness equal to the conduction length, where the conduction term in the energy balance equation is of the same magnitude as the shear production and inelastic dissipation, and where the volume fraction is not a constant. In this case, a dimensionless group can

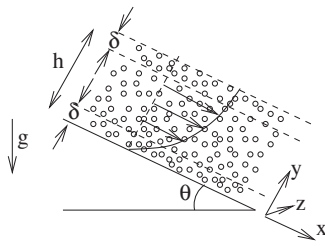


FIG. 1. Configuration and coordinate system.

be formed using the energy flux, the stress, the particle mass, and the thermal conductivity, and so the Bagnold law is no longer a dimensional necessity. In order to obtain a constant volume fraction, it is necessary to show that this energy conduction term is not important in the bulk of the flow. This issue was examined in Ref. 46, where it was shown that the rate of conduction of energy is important in boundary layers of thickness comparable to the conduction length for a dense granular flow scales as $[d/(1-e_n)^{1/2}]$, where e_n is the normal coefficient of restitution. The conduction length is large compared to the particle diameter for nearly elastic particles, but is of the same magnitude as the particle diameter for highly inelastic particles. In simulations, the thickness of the top and bottom boundary layers is usually about 3–5 particle diameters. In the present study, we focus on the bulk flow. The top 5 and bottom 5 layers in the y direction are not considered when results are reported, and only the central 30 layers are used for calculating the coordination number and the stresses in the flow.

II. SIMULATION TECHNIQUE

The granular material is composed of *monodisperse* hard particles of diameter d flowing down a plane inclined at an angle θ to the horizontal. A Cartesian coordinate system is used, where the velocity and velocity gradient are in the x and y directions, respectively, while the z direction is perpendicular to the plane of flow, as shown in Fig. 1. It should be noted that throughout the analysis, *the mass of a particle is set equal to 1 for simplicity so that the mass dimension is scaled by the particle mass*. The shear and normal stress balances are

$$(d\sigma_{xy}/dy) = -\rho g \sin(\theta), \quad (1)$$

$$(d\sigma_{yy}/dy) = \rho g \cos(\theta).$$

where g is the acceleration due to gravity. The ratio of the shear and normal stresses is a constant in the flow,

$$(\sigma_{xy}/\sigma_{yy}) = -\tan(\theta). \quad (2)$$

In the simulations, periodic boundary conditions are applied in the x and z directions, while rough particle boundary conditions¹⁰ are applied at the bottom of the flowing layer in the y direction, and there is a free surface at the top of the layer. The simulation cell contains a total of 8000 particles, with aspect ratio of 2:4:1 along the x , y , and z directions, respectively. This gives us a total height of the flowing layer of about 40 particle diameters. The simulation is started with

random initial velocities for all the particles, and the simulation is permitted to evolve until steady state is reached.

The discrete element technique is used for simulating the flow, and the particle contact models used here are the linear and Hertzian contact models. The linear contact model results in a constant coefficient of restitution for binary interactions, but the coefficient of restitution for the Hertzian contact model is velocity dependent, as discussed below. The details of the simulation technique have been discussed in detail in a previous study,¹⁰ and a brief summary is provided in Appendix A.

The linear contact model without friction can be directly compared with theory and with ED simulations with a constant coefficient of restitution since the contact time and coefficient of restitution are independent of the initial velocity. In the case of the linear contact model with no friction, we have been able to obtain a stable flow only for coefficient of restitution $e_n \leq 0.8$, while the flow for $e_n = 0.9$ was continuously accelerating. A stable flow was obtained when the angle of inclination was $21^\circ \leq \theta \leq 24^\circ$. In the case of the linear contact model with friction, we have been able to obtain a steady flow for $e_n \leq 0.9$, and we report the results for the coefficient of restitution in the range of $0.5 \leq e_n \leq 0.9$. A steady flow is obtained when the angle of inclination is in the range of $21^\circ \leq \theta \leq 25^\circ$. In the case of the Hertzian contact model, we were not able to obtain a steady flow for a reasonable range of angles of inclination without friction. Therefore, we do not report the results for the Hertzian contact model with no friction. In the case of the Hertzian contact model with friction, a steady flow was observed for $21^\circ \leq \theta \leq 25^\circ$ when the friction coefficient is set equal to 0.5. The parameters used in the DE simulations are provided in Table II.

In addition to the DE simulations, we also use the ED simulations of the simple shear flow using the Lees–Edwards boundary conditions in the absence of gravity. The procedure used is the same as that in Refs. 28 and 29. The hard particle model is used in the ED simulations, and collisions between particles are instantaneous. The purpose is to make a comparison between the local rheology in the bulk of the granular flow down an inclined plane and the rheology in a uniform homogeneous shear flow. It has already been reported⁵⁴ that rheological parameters in the bulk of the flow down an inclined plane in DE simulations are in quantitative agreement with those of a linear shear flow using DE simulations in the absence of gravity. This implies that the stresses in the bulk of the flow down an inclined plane are only a function of the local strain rate. The objective here is to compare the stresses in the DE simulations for the flow down an inclined plane, as the spring constant is increased, with the stresses for the hard particle model with instantaneous interactions. In this simulation technique, the interaction between particles are modeled as instantaneous contacts, in which the postcollisional relative velocity normal to the surface of contact is $-e_n$ times the precollisional relative normal velocity, and the postcollisional relative velocity tangential to the surface of contact is $-e_t$ times the precollisional relative tangential velocity. Here, e_n is the normal coefficient of restitution and e_t is the tangential coefficient of restitution. The tangen-

TABLE II. Parameter values used in the DE simulations. The friction coefficient was set equal to 0.5 in all simulations with friction.

Linear no friction			Linear with friction			Hertzian with friction	
$[k_n/(mg/d)]$	$[\gamma_n/(g/d)^{1/2}]$	e_n	$[k_n/(mg/d)]$	$[\gamma_n/(g/d)^{1/2}]$	e_n	$[k'_n/(mg/d^{3/2})]$	$[\gamma'_n/(g^{1/2}/d)]$
2×10^5	89.62	0.8	2×10^5	42.40	0.9	2×10^5	275
2×10^6	283.40	0.8	2×10^7	134.07	0.9	2×10^6	890
2×10^7	896.19	0.8	2×10^7	423.98	0.9	2×10^8	8900
2×10^8	2834.01	0.8	2×10^8	1340.74	0.9	2×10^5	55
2×10^5	203.01	0.6	2×10^5	272.53	0.5	2×10^6	185
2×10^6	641.97	0.6	2×10^6	861.82	0.5	2×10^8	1850
2×10^7	2030.09	0.6	2×10^7	2725.30	0.5		
2×10^8	6419.72	0.6	2×10^8	8618.15	0.5		

tial coefficient of restitution e_t is set equal to 1 in the ED simulations in order to correspond to the choice $\gamma_t=0$ in the DE simulations. The normal coefficient of restitution is calculated from Eq. (A7) for the linear force model.

The results of the DE simulations are compared with the results of event-driven hard particle simulations.^{28,29} Those simulations were carried out in a cubic box using 500 particles. All simulations were averaged over 2×10^4 collisions per particle, after an initial equilibration run that extended over a time period corresponding to 2×10^4 collisions per particle. For very small system sizes, when the system is sheared, it attains in-plane ordering for the volume fractions considered here, and the structure is not random. As the system size is increased, the ordered state becomes unstable and undergoes a transition to a random state. It is this random state that is of interest in the present analysis, so care has been taken to ensure that the structure is actually random in both ED and DE simulations. Event-driven simulations suffer from the disadvantage of numerical errors due to particle overlaps when the system becomes dense. Due to the finite numerical resolution in the computations and the round-off errors therein, the actual distance between particles at collision is not equal to the projected distance that was calculated in the event-driven algorithm. When the volume fraction is high, there are often repeated collisions involving the same particle separated by time intervals approaching the round-off errors. Due to this, there may be an overlap between two particles at a collision time comparable to the round-off errors. When the collision time is next calculated with overlapping particles, a positive collision time is not obtained because they are already overlapping. This could result in the overlaps becoming larger. This often happens at high densities, resulting in the failure of the numerical scheme. This is related to the inelastic collapse phenomenon, where an infinite number of collisions take place in finite time^{55,56} and in the two-dimensional homogeneous cooling state of a granular fluid.⁵⁷ This error can be overcome by using a more realistic velocity dependent coefficient of restitution, which goes to 1 when the relative velocity goes to 0 (Ref. 58) as predicted by theories of deformable viscoelastic particles,⁵⁹ or by switching off inelasticity if the time between collisions is smaller than a minimum value.⁶⁰ In the present analysis, we do not apply these techniques, and we report the results

only for cases where there are no particle overlaps in the ED simulations. In case there are particle overlaps, the results are discarded.

III. RESULTS

A. Contacts and coordination number

The average coordination number is the average number of particles that are in contact with a particle at any instant in time. Since the hard particle model was used in DE simulations, all interactions are instantaneous collisions and the coordination number is infinitesimally small. In the DE simulations, at every time step, the number of particles that are in contact with a particle is determined, and this is averaged over all the particles in the central region of the inclined plane flow and over time in order to obtain the average coordination number. We examine how the coordination number changes as the constants k_n and k'_n in the contact law are increased.

First, it is important to note that the coordination number is a function of height, even though the volume fraction shows very little variation with height, due to the increase in the overburden of particles deeper into the flow. This variation is shown for different angles of inclination and spring stiffnesses in Appendix B. Here, we find that the coordination number within the bulk of the flow, excluding the conduction layers with thickness of 5 particle diameters at the top and bottom, varies by about 15%. This is much larger than the variation in the volume fraction, but it is smaller than the variation expected if the coordination number increases proportional to the overburden. In the following, we show the results for the average coordination number in the bulk of the flow excluding the top and bottom 5 layers.

Figures 2–4 show the change in the coordination number as the stiffness parameters k_n and k'_n are increased over four orders of magnitude, both for linear contact law with no friction, the linear contact law with friction, and the Hertzian contact law with friction, respectively. In all cases, it is observed that the coordination number has a maximum value between 2 and 4 for the lowest angles of inclination and the lowest scaled spring stiffness of 2×10^5 used in the present simulations. However, as the spring stiffness increases, the coordination number decreases. For a scaled spring stiffness

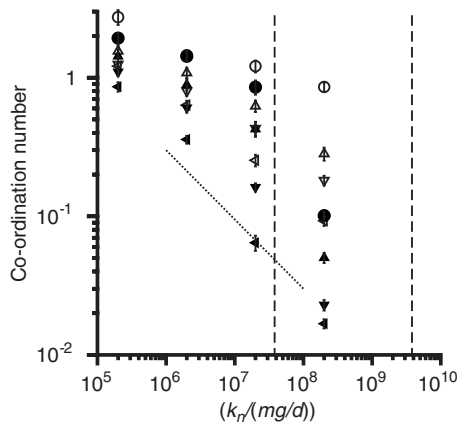


FIG. 2. Average coordination number as a function of the spring constant for the linear force model with no friction for $k_t=(2k_n/7)$, $\gamma_t=0$, and the value of γ_n chosen so that $e_n=0.8$ (filled symbols) and $e_n=0.6$ (open symbols). The angles of inclination are $\theta=21^\circ$ (\circ), $\theta=22^\circ$ (Δ), $\theta=23^\circ$ (∇), and $\theta=24^\circ$ (\triangleleft). The vertical dashed lines correspond to $[k_n/(mg/d)]=3.82 \times 10^7$ and 3.82×10^9 , which are the reference values for particles with $k_n=0.5 \times 10^6$ N/m, mass density of 2500 kg/m³, and diameter of 100 μm – 1 mm, respectively. The dotted line shows a slope of $(-1/2)$.

of 2×10^8 , the coordination number decreases below 1 in all cases, except for the lowest angle of inclination of 21° . This implies that each particle is in contact with less than 1 particle, on average, for a scaled spring stiffness of 10^8 for both linear and Hertzian models. The coordination number increases systematically as the coefficient of restitution is decreased, and it is larger when there is friction between the particles. Also shown by the vertical dashed lined in Figs. 2 and 3 (and in subsequent figures for the linear contact law) are the scaled spring constants $[k_n/(mg/d)]=3.82 \times 10^7$ and 3.82×10^9 for particles with diameters of 1 mm and 100 μm , respectively, a mass density of 2500 kg/m³, and a typical dimensional spring constant of 2×10^6 N/m (Refs. 50 and 52) for sand particles. It is clear that the coordination number for the flow of real particles is greater than 1 only at

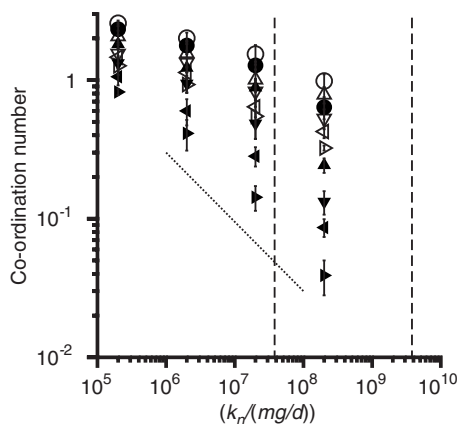


FIG. 3. Average coordination number as a function of the spring constant for the linear force model with friction ($\mu=0.5$) for ($e_t=1$, $e_n=0.9$) (filled symbols) and ($e_t=1$, $e_n=0.5$) (open symbols). The angles of inclination are $\theta=21^\circ$ (\circ), $\theta=22^\circ$ (Δ), $\theta=23^\circ$ (∇), $\theta=24^\circ$ (\triangleleft), and $\theta=25^\circ$ (\triangleright). The vertical dashed lines correspond to $[k_n/(mg/d)]=3.82 \times 10^9$ and 3.82×10^7 , which are the reference values for particles with $k_n=0.5 \times 10^6$ N/m, mass density of 2500 kg/m³, and diameter of 100 μm – 1 mm, respectively. The dotted line shows a slope of $(-1/2)$.

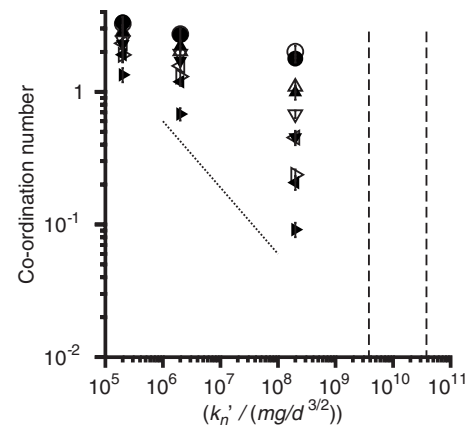


FIG. 4. Average coordination number as a function of the spring constant for the Hertzian force model with friction ($\mu=0.5$). The open symbols are for system with higher dissipation: $\{[k_n'/(mg/d^{3/2})]=2 \times 10^5$, $[\gamma_n'/(g^{1/2}/d)]=275$; $\{[k_n'/(mg/d^{3/2})]=2 \times 10^6$, $[\gamma_n'/(g^{1/2}/d)]=890$; and $\{[k_n'/(mg/d^{3/2})]=2 \times 10^8$, $[\gamma_n'/(g^{1/2}/d)]=8900$; while the filled symbols are for a system with lower dissipation: $\{[k_n'/(mg/d^{3/2})]=2 \times 10^5$, $[\gamma_n'/(g^{1/2}/d)]=55$; $\{[k_n'/(mg/d^{3/2})]=2 \times 10^6$, $[\gamma_n'/(g^{1/2}/d)]=185$; and $\{[k_n'/(mg/d^{3/2})]=2 \times 10^8$, $[\gamma_n'/(g^{1/2}/d)]=1850$. The angles of inclination are $\theta=21^\circ$ (\circ), $\theta=22^\circ$ (Δ), $\theta=23^\circ$ (∇), $\theta=24^\circ$ (\triangleleft), and $\theta=25^\circ$ (\triangleright). The vertical dashed lines correspond to $(Ed^2/mg)=3.82 \times 10^{10}$ and 3.82×10^9 , which are the reference values for particles with $E=0.5 \times 10^{11}$ N/m², mass density of 2500 kg/m³, and diameter of 100 μm – 1 mm, respectively. The dotted line shows a slope of $(-1/2)$.

the lowest angle of inclination of 21° , and it decreases below 1 for all other angles of inclination. The dashed lines in Fig. 4 shows scaled spring constants $[k_n'/(mg/d^{3/2})]=3.82 \times 10^9$ and 3.82×10^{10} , corresponding to smooth sand particles with diameters of 100 μm and 1 mm, mass density of 2500 kg/m³, and elastic modulus of 10^{11} N/m² for particles such as sand and glass beads. Even though the coordination number for the Hertzian contact model is higher than that for the linear contact model for equal values of the scaled spring constant, smooth particles that follow the Hertzian contact law have a higher scaled spring constant than rough particles that follow a linear contact law. Due to this, the trends in Fig. 4 show that the coordination number for particles with the Hertzian contact law also decreases below 1 for all angles, except the lowest angle of 21° .

The duration of an interaction between two particles is independent of the approach velocity for the linear contact model, but does depend on the relative velocity in the Hertzian model. However, from the dimensional analysis, it can be inferred that the duration of an interaction is proportional to $(m/k)^{1/2}$. If the coordination number decreases proportional to the duration of an interaction at a fixed angle of inclination, one would expect the coordination number to decrease proportional to $k^{-1/2}$ (we have assumed the particle mass is 1 without loss of generality). The dotted lines in Figs. 2–4 have a slope of $(-1/2)$. It is observed that the decrease in the coordination number is consistent with the $k^{-1/2}$ power law at all angles of inclination, except for the lowest angle of 21° , where we see little change in the coordination number as the angle of inclination is increased.

More detailed statistics of particle contacts, including the fraction of particles in simultaneous contact with 1, 2, 3, ... other particles, is provided in Appendix B. Consistent with

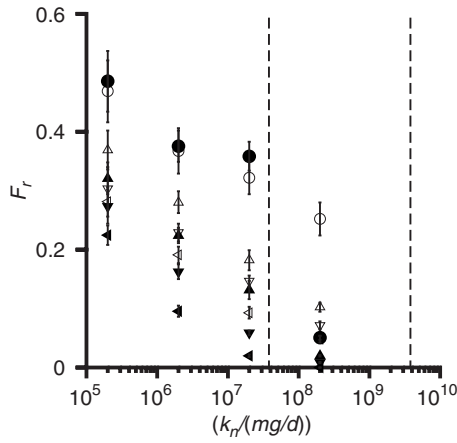


FIG. 5. The average ratio of the magnitudes of the second largest and the largest forces acting on a particle, $F_r = (|\mathbf{F}_2|/|\mathbf{F}_1|)$, as a function of the spring constant for the linear force model with no friction for $e_n=0.8$ (filled symbols) and $e_n=0.6$ (open symbols). The angles of inclination are $\theta=21^\circ$ (\circ), $\theta=22^\circ$ (Δ), $\theta=23^\circ$ (∇), and $\theta=24^\circ$ (\triangleleft). The vertical dashed lines correspond to $[k_n/(mg/d)]=3.82 \times 10^9$ and 3.82×10^7 , which are the reference values for particles with $k_n=0.5 \times 10^6$ N/m, mass density of 2500 kg/m^3 , and diameter of $100 \text{ }\mu\text{m}$ – 1 mm , respectively.

the coordination number results, we find that at the lowest angle of inclination $\theta=21^\circ$, there is little change in the number of particles with 1 and 2 contacts as the spring stiffness is increased. However, for $\theta \geq 22^\circ$, there is a systematic decrease in the number of particles with 1 or more contacts as the spring stiffness is increased, and the fraction of particles with no contacts shows a monotonic increase.

In the case of particles with multiple contacts, we can use the force ratio,¹² which is the ratio of the magnitudes of the second largest and the largest force acting on the particle at an instant. This force ratio is averaged over all the particles with two or more contacts, and over time, to get an average force ratio F_r . The force ratio and force angle are intended to provide some quantitative indication of whether there are force chains in the system. A force ratio close to 1 is a necessary, although not sufficient, requirement for force chains since there should be, at least, two instantaneous opposing forces on a single particle if stress is to be transmitted, which means that the magnitude of the two largest forces have to be nearly equal. The force angle is intended to measure whether the forces are opposing each other.

In the quasistatic limit where a particle is held in place by forces of the same magnitude from all directions, the force ratio will be close to 1. Alternatively, if there is one dominant force on the particle while all other forces are close to zero, then the force ratio will be small. Therefore, the force ratio provides an indication of whether the motion of a particle with multiple contacts is dominated by one dominant contact with a large force or whether all the forces on a particle are of the same magnitude. The force ratio is shown as a function of the angle of inclination for the linear contact model with no friction in Fig. 5, for the linear contact model with friction in Fig. 6, and for the Hertzian contact model in Fig. 7. These figures show that the force ratio decreases as the angle of inclination increases and as the coefficient of restitution increases. The force ratio has a maximum value of

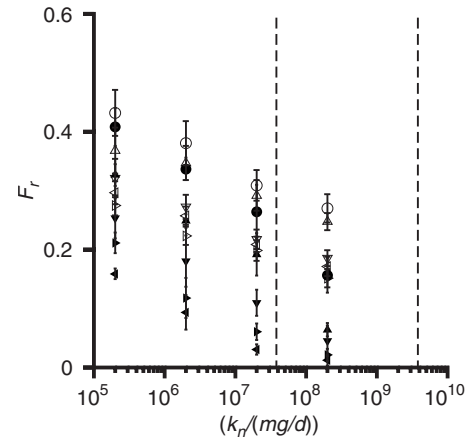


FIG. 6. The average ratio of the magnitudes of the second largest and the largest forces acting on a particle, $F_r = (|\mathbf{F}_2|/|\mathbf{F}_1|)$, as a function of the spring constant for the linear force model with friction for $e_n=0.8$ (filled symbols) and $e_n=0.6$ (open symbols). The angles of inclination are $\theta=21^\circ$ (\circ), $\theta=22^\circ$ (Δ), $\theta=23^\circ$ (∇), $\theta=24^\circ$ (\triangleleft), and $\theta=25^\circ$ (\triangleright). The vertical dashed lines correspond to $[k_n/(mg/d)]=3.82 \times 10^9$ and 3.82×10^7 , which are the reference values for particles with $k_n=0.5 \times 10^6$ N/m, mass density of 2500 kg/m^3 , and diameter of $100 \text{ }\mu\text{m}$ – 1 mm , respectively.

about 0.4 for the softest particles considered here, but it decreases below 0.3 when the angle of inclination is 21° and for scaled spring constants corresponding to materials such as sand and glass. The force ratio is less than 0.2 for higher values of the angle of inclination, indicating that there is, on average, only one dominant force on a particle. The force ratio does not also show a significant dependence on friction.

For particles with multiple contacts, the “force cosine” can be used as a measure to determine whether a particle

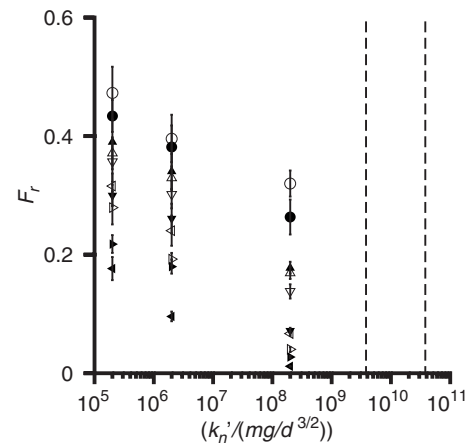


FIG. 7. The average ratio of the magnitudes of the second largest and the largest forces acting on a particle, $F_r = (|\mathbf{F}_2|/|\mathbf{F}_1|)$, as a function of the spring constant for the Hertzian contact model with friction. The open symbols are for system with higher dissipation: $\{[k_n'/(mg/d^{3/2})]=2 \times 10^5, [\gamma_n'/(g^{1/2}/d)]=275; \{[k_n'/(mg/d^{3/2})]=2 \times 10^6, [\gamma_n'/(g^{1/2}/d)]=890; \text{ and } \{[k_n'/(mg/d^{3/2})]=2 \times 10^8, [\gamma_n'/(g^{1/2}/d)]=8900; \text{ while the filled symbols are for a system with lower dissipation: } \{[k_n'/(mg/d^{3/2})]=2 \times 10^5, [\gamma_n'/(g^{1/2}/d)]=55; \{[k_n'/(mg/d^{3/2})]=2 \times 10^6, [\gamma_n'/(g^{1/2}/d)]=185; \text{ and } \{[k_n'/(mg/d^{3/2})]=2 \times 10^8, [\gamma_n'/(g^{1/2}/d)]=1850. \text{ The angles of inclination are } \theta=21^\circ (\circ), \theta=22^\circ (\Delta), \theta=23^\circ (\nabla), \theta=24^\circ (\triangleleft), \text{ and } \theta=25^\circ (\triangleright). \text{ The vertical dashed lines correspond to } (Ed^2/mg)=3.82 \times 10^{10} \text{ and } 3.82 \times 10^9, \text{ which are the reference values for particles with } E=0.5 \times 10^{11} \text{ N/m}^2, \text{ mass density of } 2500 \text{ kg/m}^3, \text{ and diameter of } 100 \text{ }\mu\text{m}$ – 1 mm , respectively.

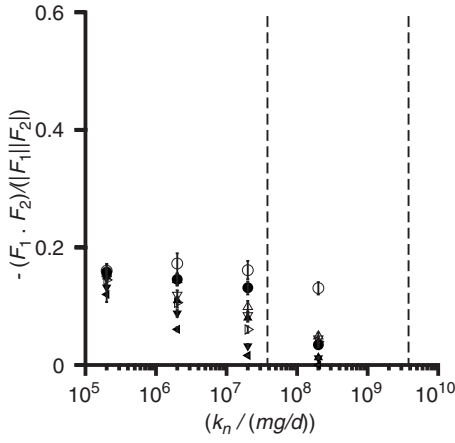


FIG. 8. The average of the force cosine, $(\mathbf{F}_1 \cdot \mathbf{F}_2) / (|\mathbf{F}_1| |\mathbf{F}_2|)$, for the two largest forces acting on a particle, for the linear force model with no friction for $e_n=0.8$ (filled symbols) and $e_n=0.6$ (open symbols). The angles of inclination are $\theta=21^\circ$ (\circ), $\theta=22^\circ$ (Δ), $\theta=23^\circ$ (∇), and $\theta=24^\circ$ (\triangleleft). The vertical dashed lines correspond to $[k_n/(mg/d)]=3.82 \times 10^9$ and 3.82×10^7 , which are the reference values for particles with $k_n=0.5 \times 10^6$ N/m, mass density of 2500 kg/m^3 , and diameter of $100 \mu\text{m}$ – 1 mm , respectively.

could be a part of a force chain as follows. Consider a particle with two contacts, in which the forces with the largest and second largest magnitude are \mathbf{F}_1 and \mathbf{F}_2 . The cosine of the angle between these two forces is given by $(\mathbf{F}_1 \cdot \mathbf{F}_2) / (|\mathbf{F}_1| |\mathbf{F}_2|)$. If the two largest forces on a particle with multiple contacts are nearly collinear, then the parameter $(\mathbf{F}_1 \cdot \mathbf{F}_2) / (|\mathbf{F}_1| |\mathbf{F}_2|)$ will be close to -1 . If $(\mathbf{F}_1 \cdot \mathbf{F}_2) / (|\mathbf{F}_1| |\mathbf{F}_2|)$ is close to zero, it indicates that there is no correlation in the alignment of the two largest forces. Since the two largest forces on the particles have to be nearly collinear for the particle to be a part of a force chain, a value of $(\mathbf{F}_1 \cdot \mathbf{F}_2) / (|\mathbf{F}_1| |\mathbf{F}_2|)$ close to -1 is a necessary (though not sufficient) condition for the presence of force chains in the system. Figure 8–10 shows the value of $(\mathbf{F}_1 \cdot \mathbf{F}_2) / (|\mathbf{F}_1| |\mathbf{F}_2|)$ for nearly elastic and highly inelastic particles for different

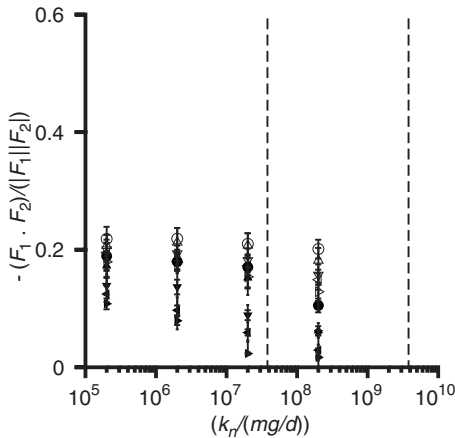


FIG. 9. The average of the force cosine, $(\mathbf{F}_1 \cdot \mathbf{F}_2) / (|\mathbf{F}_1| |\mathbf{F}_2|)$, for the two largest forces acting on a particle, for the linear force model with friction for $e_n=0.8$ (filled symbols) and $e_n=0.6$ (open symbols). The angles of inclination are $\theta=21^\circ$ (\circ), $\theta=22^\circ$ (Δ), $\theta=23^\circ$ (∇), $\theta=24^\circ$ (\triangleleft), and $\theta=25^\circ$ (\triangleright). The vertical dashed lines correspond to $[k_n/(mg/d)]=3.82 \times 10^9$ and 3.82×10^7 , which are the reference values for particles with $k_n=0.5 \times 10^6$ N/m, mass density of 2500 kg/m^3 , and diameter of $100 \mu\text{m}$ – 1 mm , respectively.

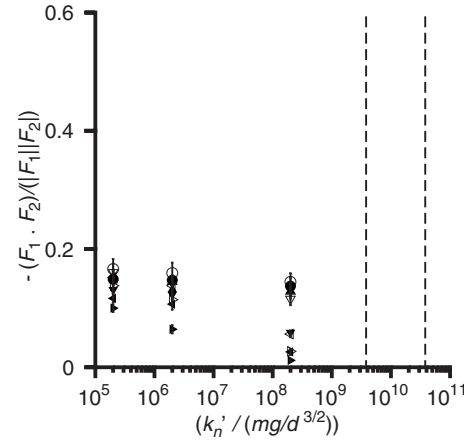


FIG. 10. The average of the force cosine, $(\mathbf{F}_1 \cdot \mathbf{F}_2) / (|\mathbf{F}_1| |\mathbf{F}_2|)$, for the two largest forces acting on a particle, for the Hertzian force model with friction. The open symbols are for system with higher dissipation: $\{[k_n'/(mg/d^{3/2})]=2 \times 10^5, [\gamma_n'/(g^{1/2}/d)]=275; \{[k_n'/(mg/d^{3/2})]=2 \times 10^6, [\gamma_n'/(g^{1/2}/d)]=890; \text{ and } \{[k_n'/(mg/d^{3/2})]=2 \times 10^8, [\gamma_n'/(g^{1/2}/d)]=8900; \text{ while the filled symbols are for a system with lower dissipation: } \{[k_n'/(mg/d^{3/2})]=2 \times 10^5, [\gamma_n'/(g^{1/2}/d)]=55; \{[k_n'/(mg/d^{3/2})]=2 \times 10^6, [\gamma_n'/(g^{1/2}/d)]=185; \text{ and } \{[k_n'/(mg/d^{3/2})]=2 \times 10^8, [\gamma_n'/(g^{1/2}/d)]=1850. \text{ The angles of inclination are } \theta=21^\circ$ (\circ), $\theta=22^\circ$ (Δ), $\theta=23^\circ$ (∇), $\theta=24^\circ$ (\triangleleft), and $\theta=25^\circ$ (\triangleright). The vertical dashed lines correspond to $(Ed^2/mg)=3.82 \times 10^{10}$ and 3.82×10^9 , which are the reference values for particles with $E=0.5 \times 10^{11} \text{ N/m}^2$, mass density of 2500 kg/m^3 , and diameter of $100 \mu\text{m}$ – 1 mm , respectively.

coefficients of restitution and for different angles of inclination for the different contact models. The force cosine is negative in all cases, indicating that there is a bias toward the opposite orientation of the two largest forces on the particles. However, the force cosine is numerically small in all cases, indicating that this bias is small. This shows that even when a particle overlaps with two other particles, there is no significant bias for the contact forces to be opposite in direction to each other, as would be required for percolating force chains in the system.

Next, we analyze the relative arrangement of particles in the flow, which is quantified by the structural order parameter Q_l , defined as

$$Q_l = \left(\frac{2l+1}{4\pi} \sum_{m=-l}^l |Y_{lm}(\theta, \phi)|^2 \right)^{1/2}, \quad (3)$$

where $Y_{lm}(\theta, \phi)$ is the spherical harmonic,

$$Y_{lm}(\theta, \phi) = \sqrt{\frac{2l+1}{4\pi}} P_l^m[\cos(\theta)] \exp(im\phi) \quad (4)$$

θ and ϕ are the azimuthal and meridional angles in a spherical coordinate system with an arbitrary axis, and P_l^m are the Legendre polynomials. For systems with perfect icosahedral ordering (fcc or bcc structures), Q_6 is greater than 0.5, whereas it is 0 for random structures. Therefore, Q_6 can be used to distinguish between random and ordered structures. For the DE simulations, the averaging in Eq. (3) is carried out over all the contacts of a particle, over all particles in the central region of the inclined plane flow, and over time. In the ED simulations, the average is carried out over collisions because particles are in contact only when there is a collision.

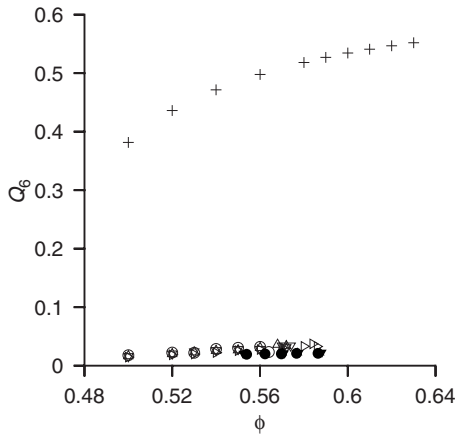


FIG. 11. The icosahedral order parameter Q_6 as a function of the volume fraction for hard inelastic particles obtained by event-driven simulations (Ref. 28) (open symbols), for the linear force model with no friction for $[k_n/(mg/d)]=2 \times 10^5$ (filled symbols), and for different coefficients of restitution $e_n=0.6$ (\circ), $e_n=0.7$ (\triangle), $e_n=0.8$ (∇), and $e_n=0.9$ (\triangleleft). The symbol + shows the icosahedral order parameter for elastic particles in the absence of shear.

sion. It should be noted that the ED simulations were carried out for a homogeneously sheared collection of spherical particles using Lees–Edwards periodic boundary conditions.

For a collection of elastic particles in the absence of shear, it is well known⁶¹ that there is a crystallization transition at a volume fraction of 0.49, after which the parameter Q_6 increases to a value between 0.5 and 0.6. In the case of shear flows of inelastic particles, ED simulations²⁸ have shown that the system remains in the disordered state even when the volume fraction is in the range of 0.5–0.6, provided the system size is sufficiently large. This indicates that mean shear has a randomizing effect on the relative arrangements of the particles in the flow. It is of interest to examine whether such a randomizing effect is observed for the bulk flow down an inclined plane in the DE simulations. The order parameter Q_6 is shown as a function of the volume fraction for scaled spring constant $[k_n/(mg/d)]=2 \times 10^5$ in Fig. 11. The values of Q_6 for all other values of the spring constant are also below 2.5×10^{-2} , indicating that there is no icosahedral order in the shear flow of soft particles down an inclined plane.

IV. GRANULAR TEMPERATURE AND DISSIPATION RATE

The “granular temperature” is defined as

$$6T = \langle m((u_x - U)^2 + u_y^2 + u_z^2) + I(\omega_x^2 + \omega_y^2 + (\omega_z - \Omega)^2) \rangle \quad (5)$$

where x , y , and z are the flow, gradient, and vorticity directions, respectively, m is the particle mass, I is the moment of inertia, U is the local mean velocity in the flow direction, and Ω is the local mean angular velocity. We also calculate the average rate of dissipation of energy per unit volume per unit time from the total energy dissipated due to particle interactions in a differential volume. In the bulk of the flow, where there is a balance between the rate of production of energy

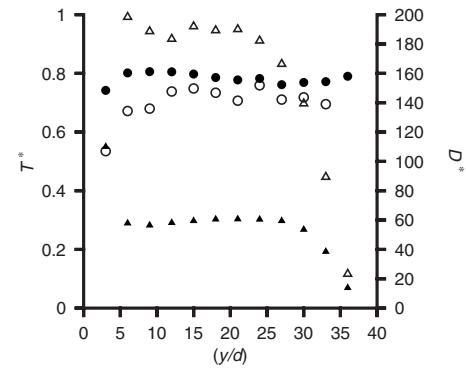


FIG. 12. The scaled temperature $T^*=(T/m\dot{\gamma}^2d^2)$ (\circ on the left y axis) and scaled dissipation rate $D^*=(Dd^4/T^{3/2})$ (\triangle on the right y axis) as a function of (y/d) , where y is the distance from the bottom of the flowing layer for the linear contact model with no friction. The open symbols show the results for angle of inclination $\theta=23^\circ$, $[k_n/(mg/d)]=2 \times 10^8$, and $e_n=0.6$, while the filled symbols show the results for $\theta=24^\circ$, $[k_n/(mg/d)]=2 \times 10^5$, and $e_n=0.8$.

due to mean shear and the rate of dissipation due to particle interactions, the hard particle model predicts that $(T/m\dot{\gamma}^2d^2)$ and $(Dd^4/m\dot{\gamma}^3)$ are constants, where T and D are the local temperature and dissipation rates, $\dot{\gamma}$ is the strain rate, and d is the particle diameter. These features have been observed earlier in the simulation of Lois *et al.*⁴⁰ and Silbert *et al.*¹⁰ This is a consequence of the absence of any material time scale in the hard particle model, due to which the only time scale is the inverse of the strain rate. We test this in the DE simulations by plotting the ratios $(T/m\dot{\gamma}^2d^2)$ and $[Dd^4/m(T/m)^{3/2}]$ in Fig. 12. In this figure, each data point is obtained by averaging over three-particle layers.

In order to validate our simulation results, we show the scaled temperature $(T/\dot{\gamma}^2d^2)$ and the scaled dissipation rate $(Dd^4/T^{3/2})$ in Fig. 12. It is observed that there is a variation of about 7% in the temperature and dissipation rate across the flow for a coefficient of restitution of 0.6, but this variation decreases as the coefficient of restitution increases. However, there is no systematic variation in the scaled temperature and dissipation rate with height, in agreement with our expectation for the hard particle model. In the following, we compare the scaled temperature $(T/m\dot{\gamma}^2d^2)$ and $[Dd^4/m(T/m)^{3/2}]$, which are obtained by averaging over the bulk of the channel for $5 \leq (y/d) \leq 33$, which the results of event-driven simulations for a homogeneous linear shear flow.^{28,29}

The variation of the temperature with volume fraction is shown in Fig. 13. The ED simulations predict that the temperature decreases as the coefficient of restitution decreases, and there is a rather sharp increase in the temperature as the ϕ_{ad} is approached. From the ED simulations, it appears that the temperatures for the different coefficients of restitution should cross since the slope of the volume fraction-temperature curves do increase as the coefficient of restitution decreases. The results of the DE simulations, in addition to being in quantitative agreement with the ED simulations, also show that the temperatures for the different coefficients of restitution do cross over. Very close to ϕ_{ad} , the temperature seems to increase as the coefficient of restitution de-

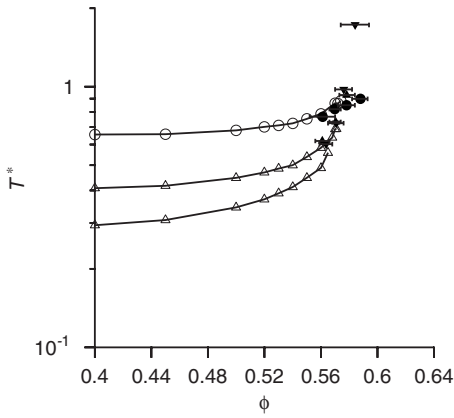


FIG. 13. The scaled temperature $T^*=(T/\dot{\gamma}^2 d^2)$ as a function of volume fraction ϕ for perfectly rough particles with tangential coefficient of restitution $e_t=1.0$ and for normal coefficient of restitution for $e_n=0.8$ (\circ), $e_n=0.7$ (\triangle), and $e_n=0.6$ (∇). The open symbols are the results of event-driven simulations for a homogeneous linear shear flow (Refs. 28 and 29), while the filled symbols are the results of DE simulations for the linear spring-dashpot model with no friction for $[k_n/(mg/d)]=2 \times 10^8$.

creases. Another puzzling feature is the apparent divergence of the temperature at the lowest coefficients of restitution considered here. It should be noted that in all the simulation results shown in Fig. 13, the temperature increases only by a factor between 4 and 5, and so a true divergence cannot be definitively inferred. However, one could speculate on the physical mechanisms, which could give rise to a divergence. The temperature is determined by a balance between the rate of production of energy due to mean shear and the rate of dissipation due to inelastic collisions. The rate of production is the product of the shear stress ($B_{xy}\dot{\gamma}^2/d$) and the strain rate, and so it is proportional to the Bagnold coefficient ($B_{xy}\dot{\gamma}^3/d$), where d is the particle diameter, and the Bagnold coefficient is a dimensionless function of the volume fraction and the coefficient of restitution. The dissipation rate (per unit volume) is proportional to $D_\phi T^{3/2} d^{-4}$, where D_ϕ is a dimensionless function of the volume fraction and coefficients of restitution. Therefore, we find that $(T/\dot{\gamma}^2 d^2) \sim (B_{xy}/D_\phi)^{2/3}$. Therefore, the temperature can diverge near ϕ_{ad} only if B_{xy} diverges faster than D_ϕ . The nature of the divergence cannot be definitively inferred from the simulation data in Fig. 13.

The scaled dissipation rate is shown in Fig. 14 for both the event-driven and the DE simulations. In this figure, the error bars in the volume fraction axis translate into significant variations in the dissipation rate because of the sharp increase in the dissipation rate with volume fraction near ϕ_{ad} . However, subject to these error bars, there is quantitative agreement between theory, ED simulations, and DE simulations.

The anisotropy in the distribution of the components of the kinetic energy in the translational and rotational modes in the bulk of the flow is shown in Fig. 15 for $e_n=0.6$. The value of $e_n=0.6$ was chosen because it exhibits the maximum departure from isotropic distribution of kinetic energy between the different modes; the distributions for higher coefficients of restitution are more isotropic. The anisotropy in the distribution of kinetic energies is small, and the ratios

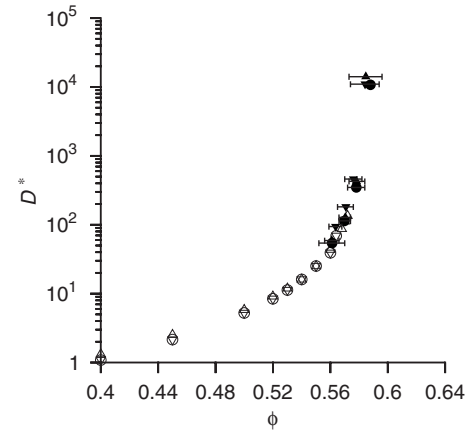


FIG. 14. The scaled dissipation rate $D^*=(Dd^4/T^{3/2})$ as a function of volume fraction ϕ for perfectly rough particles with tangential coefficient of restitution $e_t=1.0$ and for normal coefficient of restitution $e_n=0.8$ (\circ), $e_n=0.7$ (\triangle), and $e_n=0.6$ (∇). The open symbols are the results of event-driven simulations for a homogeneous linear shear flow (Refs. 28 and 29), while the filled symbols are the results of DE simulations for the linear spring-dashpot model with no friction for $[k_n/(mg/d)]=2 \times 10^8$.

$(\langle v_i^2 \rangle / T)$ and $(I\langle \omega_i^2 \rangle / T)$ vary in a small range of 0.9–1.1 for both the event-driven and the DE simulations. The mean kinetic energy in the flow direction is larger than that in the gradient and vorticity directions, while the mean rotational energy in the vorticity direction is higher than that in the other two directions in both the event-driven and DE simulations. The only exception is for the highest volume fraction in the DE simulation at an angle of inclination of 21° , where the mean kinetic energy in the flow direction seems to be less than that in the gradient and vorticity directions. There is even quantitative agreement between the DE and the event-driven simulations.

Next, we consider the relationship between the local mean angular velocity Ω_z of the particles in the vorticity direction and the local vorticity. For a linear shear flow, the symmetric and antisymmetric components of the rate of deformation tensor are equal, and so the magnitude of the vor-

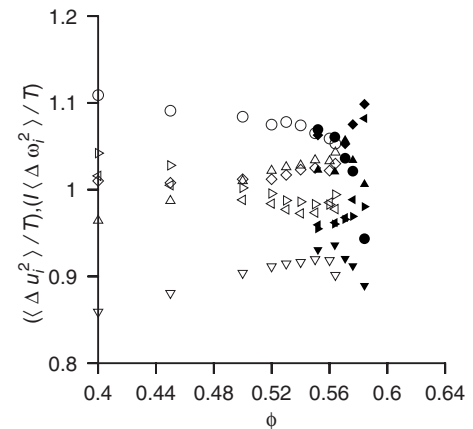


FIG. 15. The scaled mean square velocities, $(\langle (u_x - U)^2 \rangle / T)$ (\circ), $(\langle u_y^2 \rangle / T)$ (\triangle), $(\langle u_z^2 \rangle / T)$ (∇), $(I\langle \omega_x^2 \rangle / T)$ (\triangleleft), $(I\langle \omega_y^2 \rangle / T)$ (\triangleright), and $(I\langle (\omega_z - \Omega)^2 \rangle / T)$ (\diamond), as a function of volume fraction ϕ for the event-driven simulations with $e_n=0.6$ and $e_t=1$ (open symbols), and the DE simulations with $[k_n/(mg/d)]=2 \times 10^8$, $e_n=0.6$, and $e_t=1.0$ (filled symbols).

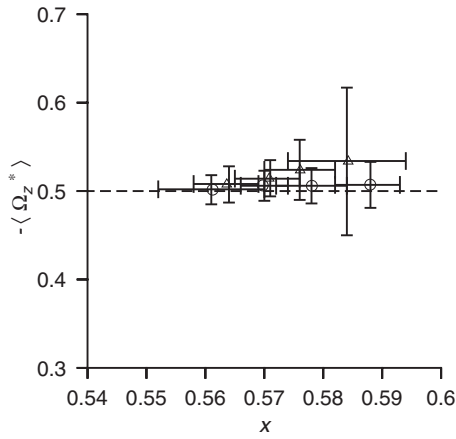


FIG. 16. The scaled average angular velocity $-\langle\Omega_z^*\rangle = -\langle(\Omega_z/\dot{\gamma})\rangle$, averaged over the central region of the flow down an inclined plane, as a function of volume fraction for the linear contact model with no friction for $e_n=0.8$ (○) and $e_n=0.6$ (△).

ticity is equal to the magnitude of the strain rate, and the direction of the vorticity vector is along the $-z$ axis. In the simulations, we find that the angular velocity Ω_z is negative (particles are rotating in the clockwise direction, on average). In Fig. 16, we show the ratio $\langle(-\Omega_z/\dot{\gamma})\rangle$, where the ratio of the local mean angular velocity and strain rate is taken, and then averaged over the central region of the flow. There are significant error bars in the calculation of both the volume fraction and the mean angular velocity. However, it is clear that the ratio is, to within simulation accuracy, equal to 0.5, indicating that the mean angular velocity of the particles is equal to the local material rotation rate. A similar result was obtained for all the other collision models used here and for all other coefficients of restitution.

V. COLLISION FREQUENCY AND RELATIVE VELOCITY DISTRIBUTION

An earlier study^{28,29} on the shear flow of inelastic hard spheres showed that there are two correlation effects that have a significant effect on the dynamics of the system. The first is in relation to the frequency of collisions between particles. It was found that the collision frequency is higher than that for a collection of elastic spheres in the absence of shear, and it diverges at a lower volume fraction than the random close packing volume fraction of 0.64. The volume fraction at which the collision frequency diverges, named the volume fraction for arrested dynamics ϕ_{ad} , decreases as the coefficient of restitution decreases, and it has a minimum value of about 0.58–0.585 for rough particles with $e_t=1.0$ and normal coefficients of restitution in the range of $e_n=0.6$ –0.8. From the sheared inelastic hard sphere simulations, it was found that the collision frequency is fitted by a function of the form

$$\nu = \frac{\nu_0}{(\phi_{ad} - \phi)^a}, \quad (6)$$

where the parameters ν_0 , ϕ_{ad} , and a , which are obtained by fitting the simulation data in the limit $\phi \rightarrow \phi_{ad}$, are shown in Table III. The collision frequency used here, which is scaled by the inverse of the strain rate, is slightly different from the

TABLE III. The parameters in the correlation equation (6) for the collision frequency for rough particles and different normal coefficients of restitution.

e_t	e_n	ϕ_{ad}	a	ν_0
1.0	0.9	0.602	1.28	2.188
1.0	0.8	0.585	1.65	0.670
1.0	0.7	0.583	1.74	0.641
1.0	0.6	0.582	1.88	0.492

scaled collision frequency in Ref. 28. The collision frequency is shown as a function of volume fraction in Fig. 17. The dashed lines in Fig. 17 show function (6), with the parameters given in Table III.

The second effect is the change in the form of the relative velocity with which particles collide. In a gas of elastic spheres in the absence of shear, the molecular chaos approximation applies and the relative velocity distribution is a Gaussian distribution with a variance equal to two times that for the single-particle distribution. For a gas of inelastic particles under shear, it was found²⁹ that the distribution for the relative velocity along the line joining centers is significantly different from a Gaussian distribution, although the distribution for the component of the relative velocity tangential to the surfaces at contact is well fitted by a Gaussian distribution. The relative velocity distribution normal to the surfaces at contact approaches an exponential distribution as the coefficient of restitution is decreased, and it is well fitted by a distribution of the form

$$f_{wn}^{(0)}(w_n) = \frac{C}{1 + e_n^{-1}} \alpha \exp(-\alpha w_n) + \frac{(1 - C)}{\sqrt{\pi T_{wn}/2(1 + e_n^{-1})}} \exp(-w_n^2/2T_{wn}), \quad (7)$$

where the parameter α is calculated from the distribution function obtained in the simulations using

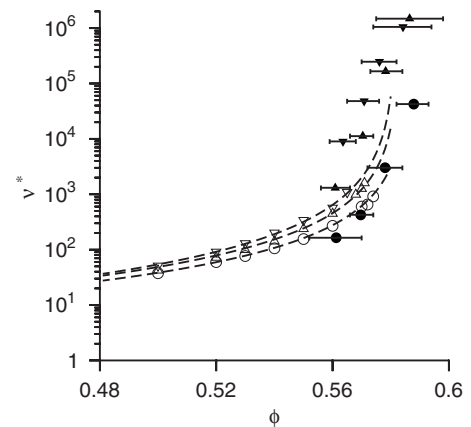


FIG. 17. The scaled collision frequency $\nu^* = (\nu/\dot{\gamma})$ as a function of volume fraction from event-driven simulations of a homogeneous linear shear flow (open symbols) and DE simulations for the flow down an inclined plane (filled symbols) for rough particles with coefficients of restitution: $e_n=0.8$, $e_t=1.0$ (○); $e_n=0.7$, $e_t=1.0$ (△); $e_n=0.6$, $e_t=1.0$ (▽). The dashed lines show the results of the empirical relation [Eq. (6)], with parameters given in Table III. In the DE simulations the spring constants are $[k_n/(mg/d)]=2 \times 10^8$, $k_t=(2k_n/7)$, damping constants $\gamma_t=0$ and γ_n adjusted to obtain the required normal coefficient of restitution. The error bars show the variation in the volume fraction in the DE simulations.

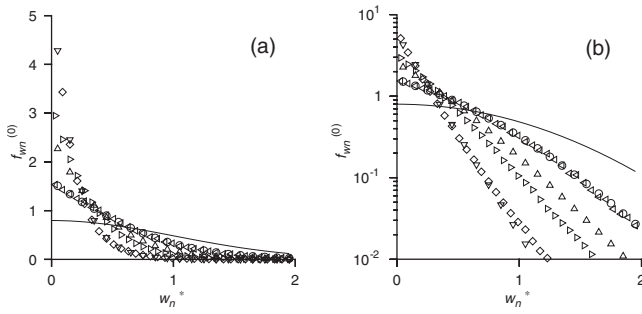


FIG. 18. The relative velocity distribution $f_{wn}^{(0)}$ as a function of the scaled relative velocity $(w_n/\sqrt{2T})$, where the temperature T is defined in Eq. (5). The open symbols show the results of event-driven simulations for $\phi=0.56$, for rough particles for coefficients of restitution: $e_n=0.8$, $e_t=1.0$ (\circ); $e_n=0.7$, $e_t=1.0$ (\triangle); and $e_n=0.6$, $e_t=1.0$ (∇). The filled symbols are the results of the DE simulations for the flow down an inclined plane spring constants $[k_n/(mg/d)]=2 \times 10^8$, $k_t=(2k_n/7)$, damping constants $\gamma_t=0$ and γ_n adjusted to obtain the required normal coefficient of restitution. The angle of inclination in the DE simulations is $\theta=23^\circ$, and the coefficients of restitution and volume fraction are (\triangleleft) $e_n=0.8$, $\phi=0.56971 \pm 0.003852$; (\triangleright) $e_n=0.7$, $\phi=0.57041 \pm 0.003981$; and (\diamond) $e_n=0.6$, $\phi=0.57084 \pm 0.005615$. (a) shows the distribution function on a linear scale, and (b) shows the same distribution on a semilog scale. The solid line shows the Gaussian distribution, and all distributions have been normalized so that the area under the curve is 1.

$$\alpha = \left[\frac{6 \int_0^\infty dw_n w_n^3 f_{wn}^{(0)}(w_n)}{\int_0^\infty dw_n w_n f_{wn}^{(0)}(w_n)} \right]^{-1/2} \quad (8)$$

and T_{wn} , the effective temperature for the normal velocity fluctuations and the translational temperature, is given by

$$T_{wn} = \left[\frac{2 \int_0^\infty dw_n w_n^3 f_{wn}^{(0)}(w_n)}{\int_0^\infty dw_n w_n f_{wn}^{(0)}(w_n)} \right] = \frac{3}{\alpha^2}. \quad (9)$$

The constant C in Eq. (7) is a fitted parameter, which is obtained by minimizing the mean square of the deviation of the actual distribution from the composite distribution (7), and is given by

$$C = 2.5(1 - e_n) \quad \text{for } e_n > 0.6 = 1.0 \quad \text{for } e_n < 0.6 \quad (10)$$

for rough particles with $e_t=1$. The parameter α was found to be fitted by an equation of the form

$$\alpha = A_\alpha \log(\phi_{ad} - \phi) + B_\alpha, \quad (11)$$

where A_α and B_α depend on the coefficient of restitution. The values of A_α and B_α given in Ref. 29 are used for comparison with event-driven simulations. The relative velocity distribution is shown for different values of the coefficient of restitution for the hard particle model in Fig. 18. It is clear that the fitting form (7) provides a good approximation for the relative velocity distribution for all values of the coefficient of restitution.

It is necessary to define the collision frequency and relative velocity distribution carefully for the soft particle DE simulations. A collision frequency cannot be defined when the system is in a multibody continuous-contact regime. We examine the collision frequency only for the highest spring constant $[k_n/(mg/d)]=2 \times 10^8$ and for angles of inclination greater than 22° , where the particle interactions are primarily through two-body contacts. At every time step t_i , we list all

the particles that overlap, determine the particles that overlap at time t_i , and compare this with particles that were overlapping at the previous time step t_{i-1} . A collision has occurred if a pair of particles, which overlaps at time step t_i , was not overlapping at time step t_{i-1} . The number of collisions is counted during the period of the simulation, and divided by the volume and the total time, to obtain the collision frequency. In order to calculate the normal relative velocity distribution, we identify all pairs of particles that overlap at time t_i , which were not overlapping at time t_{i-1} . The relative velocity of this pair of particles at the precollisional time t_{i-1} is the relative precollisional velocity of the pair of particles. The relative precollisional velocities are recorded, and the distribution of these velocities is obtained.

The collision frequency obtained as above from DE simulations is shown in Fig. 17. Although there are significant error bars in the volume fraction axis, corresponding to the fluctuations in the volume fraction in the flow down an inclined plane, it is clear that the divergence of the collision frequency is at a volume fraction lower than the random close packing volume fraction in DE simulations as well. In addition, it is clear that the volume fraction for arrested dynamics, at which the volume fraction diverges, does show a decrease with a decrease in the coefficient of restitution, similar to that in the ED simulations. This indicates that the divergence of the collision frequency in ED simulations is also observed in DE simulations.

The precollisional relative velocity distribution is shown in Fig. 18. It is not possible to compare the relative velocity distribution at equal volume fractions in DE and ED simulation because the volume fraction in DE simulations is set by the angle of inclination, and there are some fluctuations in the volume fraction. In Fig. 18, we have compared the distribution function in ED simulations for $\phi=0.56$ with those in DE simulations at an angle of inclination of 23° . In the DE simulations, we define the local scaled relative velocity as $w_n^*=(w_n/T^{1/2})$, where T is the local temperature (the temperature varies with height in the DE simulations). The velocity distribution function, expressed in terms of the local scaled relative velocity, is then averaged over the central region of the flow where the volume fraction is a constant. This averaged relative velocity distribution, shown in Fig. 18, is then compared with the results of ED simulations for a simple shear flow, where the temperature is uniform. There are clear correlation effects on the collision frequency and the relative velocity distribution in the soft particle DE simulations as well. The relative velocity distributions obtained in DE simulations are also in good quantitative agreement with those in ED simulations even though the volume fractions are not exactly the same. In particular, we clearly observe the transition from a Gaussian distribution to the exponential distribution in the DE simulations. This shows that the same correlation effects observed in hard particle systems are also present in soft particle systems when the spring constants for the interactions are sufficiently high.

VI. DYNAMICS

For a homogeneous linear shear flow, all the components of the stress are proportional to the square of the strain rate from the dimensional analysis,

$$\sigma_{ij} = B_{ij} d \dot{\gamma}^2, \quad (12)$$

where B_{ij} , the Bagnold coefficients, are functions of the volume fractions and the parameters in the contact model. In the flow down an inclined plane, Eq. (12) (Bagnold law) is still valid at the center of the flow sufficiently far from boundaries, where the rate of conduction of energy is small compared to the rates of production and dissipation. The Bagnold law is not valid in boundary layers of thickness comparable to the conduction length $\delta = [d/(1-e_n)^{1/2}]$, where the rate of conduction of energy is comparable to the rate of dissipation. In the DE simulations, we calculate the Bagnold coefficient as the ratio of the stress and square of the strain rate in the central region of the flow with thickness of about 30 particle diameters; the regions at the top and bottom with thickness of 5 particle diameters are not included in the calculation of the Bagnold coefficients. The volume fraction in the event-driven simulations is fixed by the size of the simulation cell and the number of particles, but the volume fraction in the DE simulations of the flow down an inclined plane has small variations. These variations are quantified by dividing the central region into bins of 1 particle diameter and then calculating the standard deviation over all the bins. This standard deviation is shown by the error bars in the following figures.

Since the Bagnold coefficients for the linear and Hertzian contact model with friction have been discussed before, in Ref. 10, for example, we restrict our attention to the Bagnold coefficients for the linear contact model with no friction, with the objective of comparing theory, hard particle simulations, and DE simulations. As reported earlier,^{10,12} the Bagnold coefficients B_{xx} and B_{yy} differ by less than 1%, whereas the Bagnold coefficient for the stress in the vorticity direction B_{zz} is significantly less than B_{xx} and B_{yy} . Figure 19 shows the Bagnold coefficients $B_{xx} \approx B_{yy}$, B_{zz} , and B_{xy} as a function of the volume fraction in the central region of the flow down an inclined plane. The lines show the error bars along the volume fraction axis. In all cases, it is observed that there is very little variation of the Bagnold coefficient with the spring constant k_n or with the coefficient of restitution e_n . It is clear that the Bagnold coefficients do increase as the coefficient of restitution decreases, although the increase is very small for $e_n \leq 0.8$. The Bagnold coefficients show very little variation as the spring constant in the contact model is increased. This is a very surprising feature of the flow down an inclined plane, especially since the coordination number shows a rather large variation with spring constant in this regime. In the multibody contact regime, it might be expected that the time period of an interaction is comparable to the time between interactions. In this case, the time period of an interaction $(m/k_n)^{1/2}$ should also be considered in the dimensional analysis. More specifically, if there are pervasive multibody contacts in the system, then a second particle has to come in contact with a test particle,

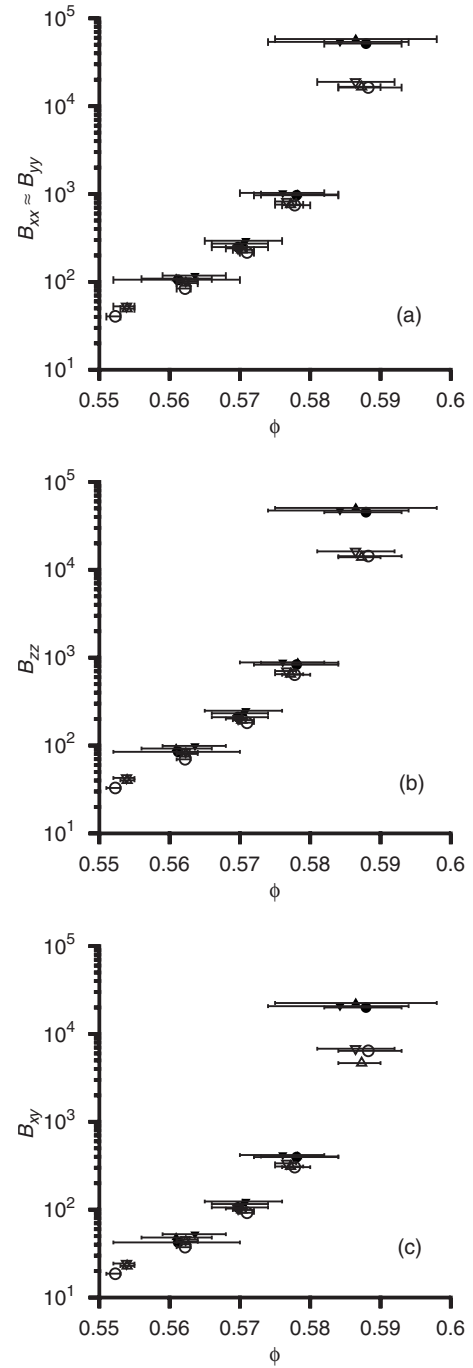


FIG. 19. The Bagnold coefficients $B_{xx} \approx B_{yy}$ (a), B_{zz} (b), and B_{xy} (c) as a function of the volume fraction from DE simulations for the flow down an inclined plane. The contact model used is the linear spring-dashpot model with no friction, scaled spring constant $[k_n/(mg/d)] = 2 \times 10^5$ (open symbols) and $[k_n/(mg/d)] = 2 \times 10^8$ (filled symbols), and for coefficients of restitution: $e_n = 0.8$ (○), $e_n = 0.7$ (△), and $e_n = 0.6$ (▽). The tangential damping constant γ_t is equal to zero, while the normal damping constant is adjusted to obtain the desired normal coefficient of restitution. The lines show the error bars along the volume fraction axis.

while it is already in contact with another particle. This implies that the time period of contact has to be comparable to the time between contacts. In a homogeneous shear flow, the maximum period of contact of two particles is the inverse of the strain rate. In this case, τ_c is also a relevant variable in the problem and should be included in the dimensional

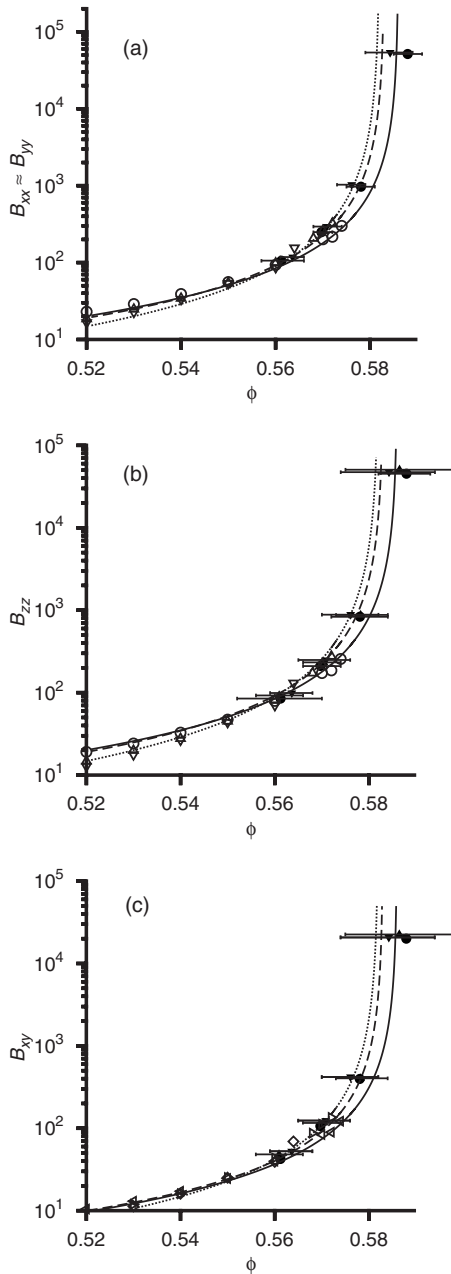


FIG. 20. The Bagnold coefficients $B_{xx} \approx B_{yy}$ (a), B_{zz} (b), and B_{xy} (c) as a function of volume fraction from DE simulations for the flow down an inclined plane (filled symbols), theory (lines), and ED simulations (open symbols) for a simple shear flow for normal coefficients of restitution: $e_n = 0.8$ (\circ), $e_n = 0.7$ (\triangle), and $e_n = 0.6$ (∇). The linear contact model with no friction is used in the DE simulations the scaled spring constant $[k_n/(mg/d)]$ is 2×10^8 , $k_t = (2k_n/7)$, $\gamma_i = 0$, and γ_n is adjusted to obtain the required normal coefficient of restitution.

analysis. Bagnold law is no longer a dimensional necessity.

The Bagnold coefficients obtained for the highest spring constant $[k_n/(mg/d)]$, are compared with the theory and the event-driven simulations of Kumaran²⁹ in Fig. 20. Due to the divergence of the collision frequency, the variation of the Bagnold coefficient with volume fraction is large for the parameter space analyzed in the DE simulations, and the small uncertainty in the volume fraction in the DE simulations translates into a rather large variation in the Bagnold coefficients in this regime. However, it can be inferred that within

the error bars in the DE simulations, there is quantitative agreement between the DE simulations, the ED simulations, and the theory for all the Bagnold coefficients. The only systematic difference between theory and DE simulations are observed at the highest volume fraction (greater than 0.58), (angle of inclination is 21°), just at the inception of flow. Our earlier analysis of the coordination number, the force ratio, and the force angles indicated that the system is in the multi-body contact regime at this angle of inclination, and so some differences between theory and DE simulations are expected. For all higher angles of inclination, there is quantitative agreement between theory and DE simulations, subject to the volume fraction uncertainties in the simulations.

A more sensitive measure is the variation of angle of inclination with the volume fraction since this is the ratio of two Bagnold coefficients, which has to remain finite as we approach the volume fraction for arrested dynamics. The variation of the volume fraction with angle of inclination is an important quantity in the context of dense granular flows down an inclined plane. A stable flow can be sustained only if the volume fraction decreases as the angle of inclination increases; if constitutive models predict that the volume fraction increases as the angle of inclination increases, then there is no possibility of a steady flow. The earliest constitutive relations obtained from the Boltzmann equation,^{3,4} using the Enskog approximation for the collision integral, predicted that the volume fraction always increases as the angle of inclination increases. This led to considerable doubts about whether constitutive relations from kinetic theory could be used, at all, for describing the flow down an inclined plane. A more detailed calculation using the Enskog approximation, which incorporated the Burnett terms in the constitutive relation,^{8,9} did predict that the volume fraction decreases as the angle of inclination increases. However, the results of these calculations were not in quantitative agreement with the simulation results using the soft particle model.¹⁰ The reason could be that this model did not include the effect of shear on the divergence of the collision frequency or the effect of correlations on the relative velocity distributions of colliding particles, which significantly affect the parameters in the constitutive relations.^{28,29} Here, we compare the present results of soft particle simulations with the latter calculations that use the hard particle model.

In Fig. 21(a), the angle of inclination as a function of the volume fraction from the ED and DE simulations is compared with the theory of Kumaran,^{28,29} with the relative velocity distribution function formulated using Eqs. (7)–(11). It can be seen that the theory predicts that the angle of inclination decreases rather sharply very close to the ϕ_{ad} , the volume fraction for arrested dynamics. The reason for this is the logarithmic divergence of the parameter α in Eq. (11). The normal stress is proportional to the second moment of the relative velocity distribution, whereas the shear stress is equal to the dissipation rate, which is proportional to the third moment of the relative velocity distribution. If α diverges, then the ratio of the third and second moments decreases to zero, and the angle of inclination predicted by the theory also goes to zero. This difficulty has already been anticipated in Ref. 29. Although a logarithmic divergence has

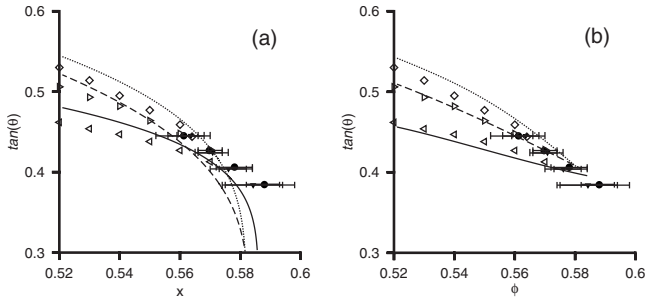


FIG. 21. The variation of the volume fraction ϕ with $\tan(\theta)$, where θ is the angle of inclination. The results of DE simulations with the linear spring-dashpot model are shown for $[k_n/(mg/d)]=2 \times 10^8$ (filled symbols) and $[k_n/(mg/d)]=2 \times 10^5$ (open symbols). In all cases, $k_t=2/7k_n$, $\gamma_t=0$, and γ_n chosen to obtain the desired normal coefficient of restitution. The values of the coefficient of restitution are $e_n=0.8$ (\circ), $e_n=0.7$ (\triangle), and $e_n=0.6$ (\diamond). The lines show the theoretical results obtained for $e_n=0.8$ (solid line), $e_n=0.7$ (dashed line), and $e_n=0.6$ (dotted line). (a) shows the theoretical results when Eq. (11) is used for the parameter α in the relative velocity distribution equation (7), while (b) shows the results when the cubic spline fit Eq. (13) is used in Eq. (7).

been proposed, it had been noted that α increases only by a factor of about 2 when the volume fraction is increased from 0.4 to the maximum value that could be simulated. This increase is too small to definitively infer a logarithmic increase, and more detailed simulations close to the volume fraction for arrested dynamics are required.

An alternative empirical form for the parameter α in Eq. (7) is to use the best spline fit using all data points for volume fractions $0.52 \leq \phi \leq \phi_{ad}$. The fit is of the form

$$\alpha = C_0 + C_1[1 - (\phi/\phi_{ad})] + C_2[1 - (\phi/\phi_{ad})]^2 + C_3[1 - (\phi/\phi_{ad})]^3. \quad (13)$$

The parameters C_0 , C_1 , C_2 , and C_3 for the best fit are provided in Table IV. Using these parameters, the theoretical predictions are shown in Fig. 21(b). Since the parameter α in Fig. 13 does not diverge, the angle of inclination tends to a finite value as the volume fraction for arrested dynamics is approached. The cubic spline fit in Fig. 21(b) seems better because the logarithmic fit in Fig. 21(a) from the DE data is very close to the volume fraction for arrested dynamics. However, the theoretical curves obtained from the logarithmic fit does represent the data well and is in error only at the highest volume fraction, which is greater than 0.58. This leads to two possibilities that have to be examined by further research. The first is that there is a logarithmic divergence of the parameter α , but as the volume fraction increases, it is not possible to observe the sharp decrease in the angle of inclination because the system transitions into a multibody contact regime. The other is that there is no true logarithmic divergence, and the angle of inclination is finite at $\phi = \phi_{ad}$.

It should be noted that the decrease of the angle of inclination to zero is a feature restricted to perfectly rough particles, where there is no dissipation of energy due to the relative tangential velocity of the particles.^{28,29} There is dissipation of energy due to relative tangential motion, which is not dependent on the parameter α in the expression for the relative normal velocity (7). Due to this, the ratio of the shear stress (equal to dissipation rate) and the normal stress will

TABLE IV. Parameters C_0 , C_1 , C_2 , and C_3 in Eq. (13) for the data of Kumaran (Ref. 29) for different values of the coefficient of restitution from the rough particle model.

e_n	C_0	C_1	C_2	C_3
0.8	1.670 16	-1.947 8	-6.443 72	50.4024
0.7	2.839 84	-7.896 39	25.458 6	-62.9158
0.6	4.481 84	-21.286 4	141.291	-417.005

remain finite as the volume fraction for arrested dynamics is approached, and the angle of inclination will be finite in this limit.

VII. CONCLUSIONS

From our analysis, it is clear that the coordination number in a dense granular flow down an inclined plane is strongly dependent on the spring stiffness in the particle model used. When the scaled spring stiffness in the linear contact model is 2×10^5 , the coordination number is less than 1 for angles of inclination in the range of $21^\circ \leq \theta \leq 24^\circ$. In contrast, when the scaled spring stiffness is 2×10^8 , the coordination number is greater than 1 only for $\theta = 21^\circ$, while it is less than 1 at higher angles of inclination. Our estimates indicate that the scaled spring constants are in the range of $10^8 - 10^{10}$ for real materials, such as sand particles, with diameters in the range of 0.1–1 mm. In the case of the Hertzian contact model, the coordination number in the range of $2 \times 10^5 \leq [k'_n/(mg/d^{3/2})] \leq 2 \times 10^8$ is larger than that for the linear contact model with spring stiffness in the range of $2 \times 10^5 \leq [k_n/(mg/d)] \leq 2 \times 10^8$. However, the scaled spring stiffness for sand grains in the diameter range of 0.1–1 mm is in the range of $10^{10} \leq [k'_n/(mg/d^{3/2})] \leq 10^{11}$. Therefore, we obtain the same conclusion that the coordination number is greater than 1 only for $\theta = 21^\circ$ and is larger than 1 for higher values of the angle of inclination. This is reinforced by our finding that the fraction of particles with two or more contacts is small, typically less than 0.15, for $\theta > 21^\circ$, and most particles have either no contacts or one contact.

An attempt was made to examine the force correlations in the particles with two or more contacts using two measures. The first is the force ratio, which is the average of the ratio of the magnitudes of the largest and second largest forces in the system. The second is the force angle, which is the angle between the two largest forces. These measures were specifically designed to test whether a large proportion of particles with two or more contacts were part of force chains propagating through the system. Since force is transmitted nearly linearly along a force chain, the two largest forces on a particle will be nearly of equal magnitude and they will be nearly collinear. Our results show that the force ratio is small, typically less than 0.2, and the force angle measure indicates that there is no biasing toward a nearly collinear orientation of the largest force. Thus, we do not see any evidence of force chains among particles with two or more contacts.

In the context of recent works on sheared inelastic hard particle fluids,^{28,29} we examined two other effects in the soft particle simulations, which have a significant effect on the dynamics of the system. The first is the divergence of the collision frequency at the volume fraction of arrested dynamics ϕ_{ad} , which is lower than the random close packing volume fraction $\phi=0.64$ for an elastic fluid at equilibrium. In sheared inelastic fluids of hard particles, the collision frequency diverges at a volume fraction in the range of 0.58–0.59 when the normal coefficient of restitution is less than about 0.8. This effect could be tested in DE simulations only for the highest scaled spring stiffness $[k_n/(mg/d)]=2 \times 10^8$ used here and for angles of inclination $\theta > 21^\circ$, where the system is mostly in the binary contact regime. Quantitative agreement was found for the collision frequency between the hard disk (event-driven) and the DE simulations if the linear contact model with no friction is used, and the damping constant in the DE simulations is adjusted to obtain the same normal coefficient of restitution as that in the event-driven simulation. The DE simulations showed that the collision frequency does diverge at a volume fraction ϕ_{ad} , which is lower than the volume fraction for random close packing.

The other correlation effect examined was the distribution of relative velocities normal to the surfaces at contact. This is important in determining the dynamics of the system since stress is transmitted primarily by collision in the dense flow regime. In a gas of elastic particles at equilibrium, the distribution of the normal relative velocities is a Gaussian distribution, with a variance equal to two times that of the single-particle velocity. A previous study using event-driven simulations²⁹ of sheared inelastic hard particles showed that the relative velocity distribution is close to a Gaussian for nearly elastic particles but undergoes a transition to an exponential distribution when the normal coefficient of restitution decreases below about 0.8. The variance of the relative velocity distribution is also much smaller than that for the single-particle distribution. Here, the relative velocity distribution has been examined in DE simulations for the linear contact model with no friction and with $[k_n/(mg/d)]=2 \times 10^8$. The results for the distribution function are in quantitative agreement with the results of the hard particle simulations²⁹ if the damping constant in the DE simulations is adjusted to obtain the same coefficient of restitution as that used in the event-driven simulations. This shows that the correlation effects observed in the hard particle model are also observed in soft particle simulations provided the spring constant is sufficiently high.

The Bagnold coefficients obtained from the DE simulations were compared to those obtained in the event-driven simulations, as well as those obtained using a theoretical calculation that takes into account the effect of correlations on the relative velocity distribution. The results were found to be in quantitative agreement. The variation of the volume fraction with the angle of inclination was also examined and found to be in quantitative agreement with hard particle simulations. For example, for a volume fraction $\phi=0.56$ (the highest volume fraction accessible in the event-driven simulations), there is a difference of less than 1° between the

angles of inclination obtained from the DE and event-driven simulations.

There was also agreement between DE simulations and theory for most volume fractions analyzed here. However, there are differences when the volume fraction is very close to the volume fraction of dynamical arrest ϕ_{ad} . This difference can be traced back to the form of the relative velocity distribution in Eq. (7), with the parameter α given by Eq. (11). Based on the available data, a cautious prediction was made in Ref. 29 that α diverges logarithmically as ϕ_{ad} is approached. It should be noted that a logarithmic divergence is very difficult to discern in event-driven simulations because it is difficult to get very close to ϕ_{ad} in simulations due to numerical errors resulting in particle overlaps. So it is difficult to definitively conclude that this slow divergence exists.

If the divergence does exist, it can be intuitively understood as the decrease to zero of the relative velocity of pairs of particles as the static configuration is approached. However, this implies that the pressure diverges faster than the rate of dissipation of energy as ϕ_{ad} is approached. This is because the collisional pressure is proportional to the second moment of the relative velocity distribution, while the rate of dissipation of energy is proportional to the third moment. From the energy balance, the shear stress is equal to the rate of dissipation of energy when the strain rate is set equal to 1. Therefore, the ratio of the shear stress and the square of the strain rate shows a sharp decrease to zero as ϕ_{ad} is approached.

More work is required to resolve whether the parameter α does diverge as ϕ_{ad} is approached. It is possible that there is a divergence, in which case the hard particle model predicts the angle of repose (the angle of inclination at which $\phi=\phi_{ad}$) is zero. This may not be seen in soft particle simulations because the system transitions to a multibody contact regime before this volume fraction is approached. Alternatively, it is possible that there is no real divergence, in which case the angle of repose (the angle of inclination at which $\phi=\phi_{ad}$) approaches a finite value. It should be noted that the decrease of the angle of repose to zero is specific to the case where there is no tangential dissipation; in the case of tangential dissipation, both the pressure and the dissipation rate will diverge as ϕ_{ad} is approached, leading to a finite angle of repose.

Apart from the above, there is another issue that requires additional work, which is the remarkable insensitivity of the Bagnold coefficients to the spring stiffness used in the simulations. We find that the Bagnold coefficients change by less than 10% when the spring stiffnesses are changed by an order of magnitude. One possible reason is that even when a particle has multiple contacts, there is one dominant contact with the largest contact force. Due to this, the system may resemble a hard particle fluid even though there are multiple contacts. Our calculations on the force ratio and the force angle does support this conclusion, but more work needs to be done.

In conclusion, it is clear that the dynamics of the flow down an inclined plane for real materials, such as sand, can be captured by hard particle models, both at the macroscopic

level (Bagnold coefficients) and the microscopic level (coordination number, icosahedral order parameter, collision frequency, and relative velocity distributions), with the exception for a very small range of angles of inclination (of about 1°) above the angle of repose. Quantitative predictions are obtained from the kinetic theory approach that incorporates the effect of shear on the collision frequency and the effect of correlations on the distribution of the relative velocities of colliding particles.

ACKNOWLEDGMENTS

This research was supported by the J. C. Bose Fellowship, Department of Science and Technology, Government of India.

APPENDIX A: FORCE MODELS AND SIMULATION TECHNIQUE

The DE technique is used for simulating the flow, and the particle contact models used here are the linear and Hertzian contact models. The linear contact model results in a constant coefficient of restitution for binary interactions, but the coefficient of restitution for the Hertzian contact model is velocity dependent, as discussed below. The details of the simulation technique have been discussed in detail in the previous study,¹⁰ and so we provide only a brief summary here.

Consider two particles i and j with positions \mathbf{r}_i and \mathbf{r}_j , linear velocities \mathbf{v}_i and \mathbf{v}_j , and angular velocities ω_i and ω_j . The overlap between the two particles is given by $\delta_{ij}=d-|\mathbf{r}_{ij}|$. There is a force between the two particles, i and j , only if δ_{ij} is less than zero, i.e., only if the particles overlap. For overlapping particles, we also define the ‘‘tangential displacement’’ \mathbf{u}_{ij}^t , which is the total displacement of the particles in the direction perpendicular to the line joining centers since the initiation of contact. For calculating the contact forces, the particle velocities are resolved along the line joining centers, $\mathbf{r}_{ij}=\mathbf{r}_i-\mathbf{r}_j$, and in the plane perpendicular to the line joining centers. The relative velocities in these two directions are

$$v_{ij}^n = (\mathbf{v}_i - \mathbf{v}_j) \cdot \hat{\mathbf{r}}_{ij}, \quad (\text{A1})$$

$$\mathbf{v}_{ij}^t = (\mathbf{I} - \hat{\mathbf{r}}_{ij}\hat{\mathbf{r}}_{ij}) \cdot \left[\mathbf{v}_i - \mathbf{v}_j - \frac{1}{2}\mathbf{r}_{ij} \times (\omega_i + \omega_j) \right], \quad (\text{A2})$$

where $\hat{\mathbf{r}}_{ij}=(\mathbf{r}_{ij}/|\mathbf{r}_{ij}|)$. The contact force acting on particle i can be resolved into a component along the line joining centers, $F_i^n \hat{\mathbf{r}}_{ij}$, and a component perpendicular to the line joining centers, \mathbf{F}_i^t ,

$$\mathbf{F}_i = F_i^n \hat{\mathbf{r}}_{ij} + \mathbf{F}_i^t. \quad (\text{A3})$$

The force on particle j is equal in magnitude and opposite in direction to the force on particle i .

For a linear force model, the normal and tangential force components are given by

$$F_i^n = k_n \delta_{ij} \hat{\mathbf{r}}_{ij} - \gamma_n m_{\text{eff}} v_{ij}^n \quad (\text{A4})$$

and

$$\mathbf{F}_i^t = k_t \mathbf{u}_{ij}^t - \gamma_t m_{\text{eff}} \mathbf{v}_{ij}^t. \quad (\text{A5})$$

In this case, the spring constants k_n and k_t have dimensions of MT^{-2} , where M and T are the mass and time dimensions, while the damping constants γ_n and γ_t have dimensions of T^{-1} . The results are analyzed in terms of the nondimensional spring constants $[k_n/(mg/d)]$ and $[k_t/(mg/d)]$ in our simulations. For simplicity, the ratio (k_t/k_n) is maintained at a constant value of $(2/7)$ in all the results used here. The dependence of the results on the ratio (k_t/k_n) has been discussed in detail in Ref. 21. The Poisson ratio of most materials is $(2/3)$, and so a value of $(k_t/k_n)=2/7$ ensures that the period of the normal and shear oscillations are equal to each other at contact for the linear model. Changing this ratio does change the kinetic energy, but not the other dynamical quantities. Therefore, we have used the ratio $(k_t/k_n)=2/7$ in all our studies.

For a binary interaction between two particles, the time period of an interaction is

$$t_c = \pi[(2k_n/m) - (\gamma_n^2/4)]^{-1/2}, \quad (\text{A6})$$

independent of the preinteraction relative velocities of the particles in the linear force model. In addition, the normal coefficient of restitution for a binary interaction e_n , which is the ratio of the post- and preinteraction relative normal velocities of the particles, is a constant, independent of the relative velocity

$$e_n = \exp(-\gamma_n t_c/2). \quad (\text{A7})$$

The above relation is used to make a connection between the DE simulations and the event-driven simulations discussed later. For simplicity, we set the tangential dissipation constant γ_t equal to zero in all our simulations; this corresponds to a tangential coefficient of restitution $e_t=1$ in the event-driven simulations.

For the Hertzian force model, the normal and tangential force components are given by

$$F_i^n = \delta_{ij}^{1/2} (k'_n \delta_{ij} - \gamma'_n m_{\text{eff}} v_{ij}^n) \quad (\text{A8})$$

and

$$\mathbf{F}_i^t = \delta_{ij}^{1/2} (k'_t \mathbf{u}_{ij}^t - \gamma'_t m_{\text{eff}} \mathbf{v}_{ij}^t). \quad (\text{A9})$$

In this case, the constants k'_n and k'_t have dimensions of $ML^{-1/2}T^{-2}$, while the damping constants γ'_n and γ'_t have dimensions $L^{-1/2}T^{-1}$. The results are expressed in terms of the dimensionless spring constant $[k'_n/(mg/d^{3/2})]$. As in the linear contact model, we set $(k'_t/k'_n)=(2/7)$ and $\gamma'_t=0$ for the Hertzian contact model as well. The time period of an interaction and the coefficient of restitution for binary interactions are velocity dependent for the Hertzian contact model. From simple dimensional analysis, it can be concluded that the average period of a binary interaction scales as $(k'_n d^{1/2}/m)^{-1/2}$.

After the force is calculated, the equations of motion are integrated to find the particle locations and velocities at each time step. The time step in the simulations for the linear contact model was 0.02 times the collision time [Eq. (A6)]. For the Hertzian contact model, the time step was 0.02 times the time obtained in Eq. (A6), with $(k'_n d^{1/2})$ substituted for k_n and $\gamma'_n d^{1/2}$ substituted for γ_n in the expression. The linear

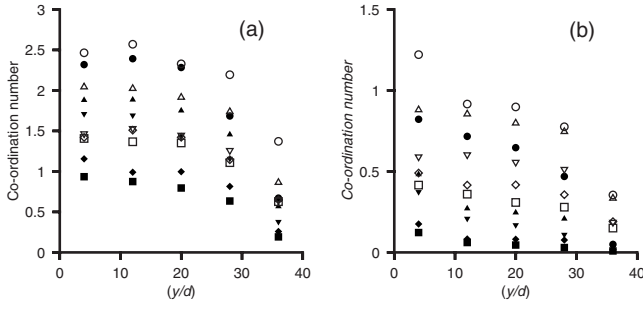


FIG. 22. Average coordination number as a function scaled height (y/d) for (a) $[k_n/(mg/d)]=2 \times 10^5$ and (b) $[k_n/(mg/d)]=2 \times 10^8$, for the linear force model with friction for $k_t=(2k_n/7)$, $\gamma_t=0$, and for the value of γ_n chosen so that $e_n=0.5$ (open symbols) and $e_n=0.9$ (filled symbols). The angles of inclination are $\theta=21^\circ$ (\circ), $\theta=22^\circ$ (\triangle), $\theta=23^\circ$ (∇), $\theta=24^\circ$ (\diamond), and $\theta=25^\circ$ (\square). The vertical dashed lines correspond to $[k_n/(mg/d)]=3.82 \times 10^9$ and 3.82×10^7 , which are the reference values for particles with $k_n=0.5 \times 10^6$ N/m, mass density of 2500 kg/m³, and diameter of $100 \mu\text{m}$ – 1 mm, respectively.

model has been implemented both with and without a friction (static yield) criterion. When there is no friction, there is no condition on the ratios of the magnitudes of the tangential and normal forces. When there is friction, the tangential displacement \mathbf{u}_{ij}^t is adjusted so that the local yield criterion, $|\mathbf{F}_{ij}^t| \leq \mu \mathbf{F}_{ij}^n$, is always satisfied, where μ is the friction coefficient. In the present case, μ has been set equal to 0.5 for all the simulations with friction. In all the simulation results, we have calculated error bars by dividing the simulation runs for production into four equal intervals and calculating the averages in each of these intervals.

In the simulations, the particles are sequentially dropped into the simulation box in which the y axis is aligned with the gravitational direction. Once the requisite number of particles has been collected in the box, the bottom two layers are “frozen,” i.e., their locations are fixed, in order to create a rough base. The direction of gravitational acceleration is then tilted to the desired angle, and the initialization continues until the system reaches the steady state. The steady state configuration is stored and used as the initial condition for calculating averages. The number of time steps for equilibration was 2×10^7 time steps for $[k_n/(mg/d)]=2 \times 10^5$ (linear model) and $[k_n'/(mg/d^{3/2})]=2 \times 10^8$ (Hertzian model), and 3×10^8 time steps for $[k_n/(mg/d)]=2 \times 10^8$ (linear model) and

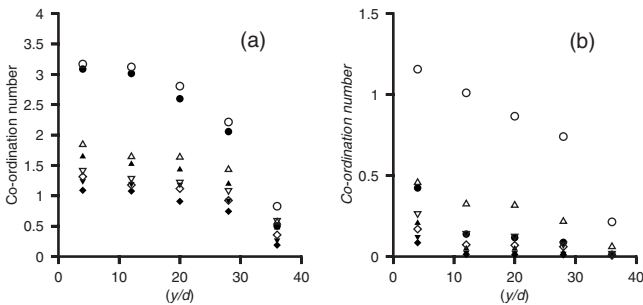


FIG. 23. Average coordination number as a function scaled height (y/d) for (a) $[k_n/(mg/d)]=2 \times 10^5$ and (b) $[k_n/(mg/d)]=2 \times 10^8$, for the linear force model without friction for $k_t=(2k_n/7)$, $\gamma_t=0$, and for the value of γ_n chosen so that $e_n=0.6$ (open symbols) and $e_n=0.8$ (filled symbols). The angles of inclination are $\theta=21^\circ$ (\circ), $\theta=22^\circ$ (\triangle), $\theta=23^\circ$ (∇), and $\theta=24^\circ$ (\diamond).

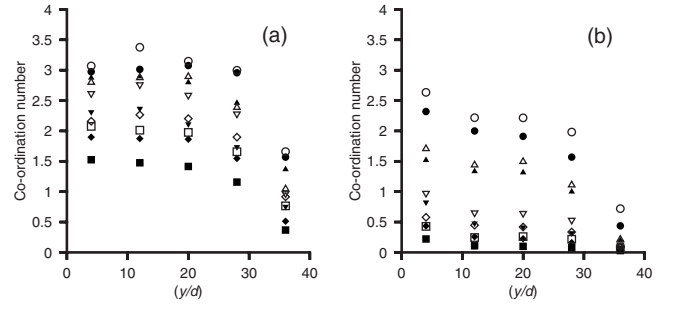


FIG. 24. Average coordination number as a function scaled height (y/d) for (a) $[k_n'/(mg/d^{3/2})]=2 \times 10^5$ and (b) $[k_n'/(mg/d^{3/2})]=2 \times 10^8$, and for the Hertzian force model with friction for $k_t'=(2k_n'/7)$, $\gamma_t'=0$. The open symbols are for higher dissipation, $\{[k_n'/(mg/d^{3/2})]=2 \times 10^8$, $[\gamma_n'/(g^{1/2}/d)]=1850$ in (a) $\{[k_n'/(mg/d^{3/2})]=2 \times 10^8$, $[\gamma_n'/(g^{1/2}/d)]=8900$ in (b), while the filled symbols are for lower dissipation, $\{[k_n'/(mg/d^{3/2})]=2 \times 10^5$, $[\gamma_n'/(g^{1/2}/d)]=275$ in (a) and $\{[k_n'/(mg/d^{3/2})]=2 \times 10^5$, $[\gamma_n'/(g^{1/2}/d)]=55$. The angles of inclination are $\theta=21^\circ$ (\circ), $\theta=22^\circ$ (\triangle), $\theta=23^\circ$ (∇), $\theta=24^\circ$ (\diamond), and $\theta=25^\circ$ (\square).

$[k_n'/(mg/d^{3/2})]=2 \times 10^8$ (Hertzian model). Statistics was collected for 10^7 time steps for $[k_n/(mg/d)]=2 \times 10^5$ (linear model) and $[k_n'/(mg/d^{3/2})]=2 \times 10^5$ (Hertzian model), and 2×10^7 time steps for $[k_n/(mg/d)]=10^8$ (linear model) and $[k_n'/(mg/d^{3/2})]=2 \times 10^8$ (Hertzian model). The standard deviation about the mean is then calculated, and the error bars in the figures have length equal to two times the standard deviation. In the coordination number, force ratio, and force angle measurements, the standard deviation is typically 10%

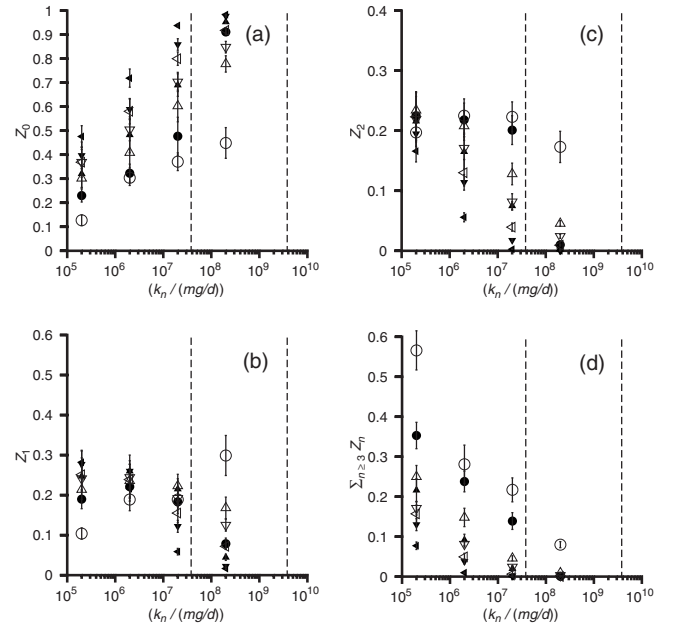


FIG. 25. The fraction Z_n of particles with n contacts, Z_0 (a), Z_1 (b), Z_2 (c), and $\sum_{n=3} Z_n$ (d), as a function of the scaled spring constant $[k_n/(mg/d)]$ for the linear contact law with no friction for $k_t=(2k_n/7)$, $\gamma_t=0$, and the value of γ_n chosen so that $e_n=0.8$ (filled symbols) and $e_n=0.6$ (open symbols). The angles of inclination are $\theta=21^\circ$ (\circ), $\theta=22^\circ$ (\triangle), $\theta=23^\circ$ (∇), and $\theta=24^\circ$ (\diamond). The vertical dashed lines correspond to $[k_n/(mg/d)]=3.82 \times 10^9$ and 3.82×10^7 , which are the reference values for particles with $k_n=0.5 \times 10^6$ N/m, mass density of 2500 kg/m³, and diameter of $100 \mu\text{m}$ – 1 mm, respectively.

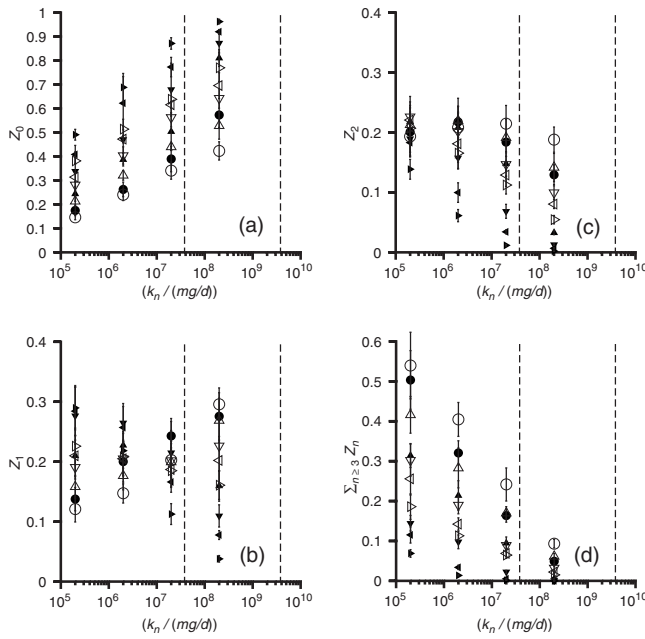


FIG. 26. The fraction of Z_n of particles with n contacts, Z_0 (a), Z_1 (b), Z_2 (c) and $\sum_{n \geq 3} Z_n$ (d), as a function of the scaled spring constant $[k_n/(mg/d)]$ for the linear contact law with friction for $k_i = (2k_n/7)$, $\gamma_i = 0$, and the value of γ_n chosen so that $e_n = 0.9$ (filled symbols) and $e_n = 0.5$ (open symbols). The angles of inclination are $\theta = 21^\circ$ (\circ), $\theta = 22^\circ$ (\triangle), $\theta = 23^\circ$ (∇), $\theta = 24^\circ$ (\triangleleft), and $\theta = 25^\circ$ (\triangleright). The vertical dashed lines correspond to $[k_n/(mg/d)] = 3.82 \times 10^9$ and 3.82×10^7 , which are the reference values for particles with $k_n = 0.5 \times 10^6$ N/m, mass density of 2500 kg/m^3 , and diameter of $100 \mu\text{m} - 1 \text{ mm}$, respectively.

of the average, while in the measurements of the fractions of particles with a specified number of contacts, the standard deviation is about 15% of the average.

APPENDIX B: PARTICLE CONTACT STATISTICS

The variation of the coordination number with (y/d) is shown in Fig. 22 for the linear contact model with friction, and in Fig. 23 for the linear contact model without friction, for two different values of the scaled spring constant, $[k_n/(mg/d)] = 2 \times 10^5$ and $[k_n/(mg/d)] = 2 \times 10^8$. Figure 24 shows the variation of the coordination number with height for the Hertzian contact model with friction for $[k'_n/(mg/d^{3/2})] = 2 \times 10^5$ and $[k'_n/(mg/d^{3/2})] = 2 \times 10^8$. In order to analyze this variation, the y coordinate was divided into five bins of width eight particle diameters each, and the coordination number was calculated in each of these bins. The lowest bin also included the two layers of frozen particles, which are neglected in the coordination number calculation. However, it is likely that the coordination number in the lowest bin is different because the coordination number between the frozen and the moving particles will, in general, be different from that between the moving particles higher up. The coordination number in the highest bin also includes the fluidized layer of particles at the top, and so the coordination number is significantly lower than the average. In addition, it is known that there are conduction boundary layers at the bottom and top of thickness $[d/(1-e_n)]^{1/2}$,⁴⁶ where the Bagnold scaling is not valid. For this reason, we do not include the top and bottom 5 layers in the calculation

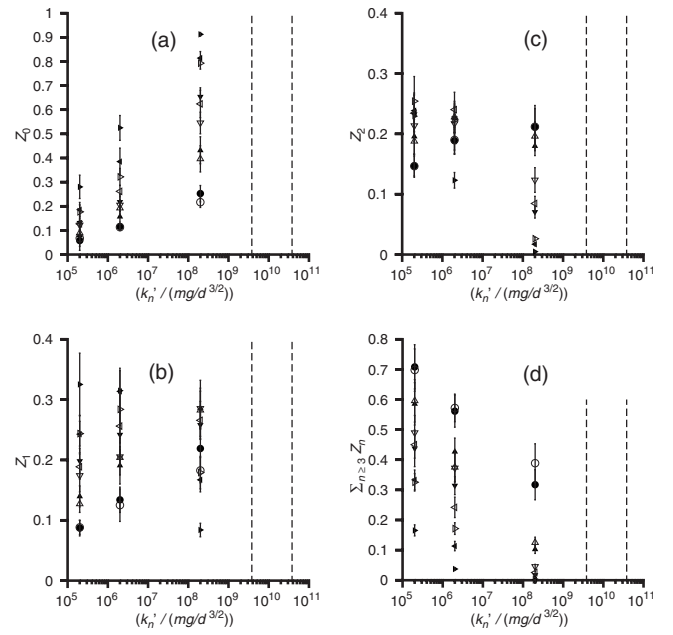


FIG. 27. The fraction Z_n of particles with n contacts, Z_0 (a), Z_1 (b), Z_2 (c), and $\sum_{n \geq 3} Z_n$ (d), as a function of the scaled spring constant $[k'_n/(mg/d^{3/2})]$ for the Hertzian contact law with friction for $k'_i = (2k'_n/7)$, $\gamma'_i = 0$. The open symbols are for system with higher dissipation: $\{[k'_n/(mg/d^{3/2})] = 2 \times 10^5, [\gamma'_n/(g^{1/2}/d)] = 275; \{[k'_n/(mg/d^{3/2})] = 2 \times 10^6, [\gamma'_n/(g^{1/2}/d)] = 890; \text{ and } \{[k'_n/(mg/d^{3/2})] = 2 \times 10^8, [\gamma'_n/(g^{1/2}/d)] = 8900; \text{ while the filled symbols are for a system with lower dissipation: } \{[k'_n/(mg/d^{3/2})] = 2 \times 10^5, [\gamma'_n/(g^{1/2}/d)] = 55; \{[k'_n/(mg/d^{3/2})] = 2 \times 10^6, [\gamma'_n/(g^{1/2}/d)] = 185; \text{ and } \{[k'_n/(mg/d^{3/2})] = 2 \times 10^8, [\gamma'_n/(g^{1/2}/d)] = 1850. \text{ The angles of inclination are } \theta = 21^\circ$ (\circ), $\theta = 22^\circ$ (\triangle), $\theta = 23^\circ$ (∇), $\theta = 24^\circ$ (\triangleleft), and $\theta = 25^\circ$ (\triangleright). The vertical dashed lines correspond to $(Ed^2/mg) = 3.82 \times 10^{10}$ and 3.82×10^9 , which are the reference values for particles with $E = 0.5 \times 10^{11} \text{ N/m}^2$, mass density of 2500 kg/m^3 , and diameter of $100 \mu\text{m} - 1 \text{ mm}$, respectively.

of averages and only include particles from $(y/d) = 5$ to $(y/d) = 35$. In this region, there is a variation of about $\pm 10\% - 15\%$ in the coordination number. A similar variation is also observed for the linear contact model without friction and the Hertzian contact model. The earlier studies of Silbret *et al.*³⁷ and Brewster *et al.*³⁸ showed a similar lack of variation of contact lifetimes with height.

A more detailed picture of the nature of particle contacts is obtained by looking at Z_n , the fraction of the total number of particles which have n contacts, where n varies from 0 (for particles that are not in contact with any other particles) to a maximum of 12 for particles arranged in a perfect fcc or hcp lattice, or even larger if the particles are severely deformed. The normalization condition requires that $\sum_0^\infty Z_n = 1.0$. The value of Z_1 (fraction of particles that overlap with one other particle), Z_2 (fraction of particles that overlap with two other particles), and $\sum_{n > 3} Z_n$ (fraction of particles that overlap with three or more other particles) for different values of the spring constant and for different angles of inclination are shown in Figs. 25–27 for the three different contact models.

There are several interesting features in these figures. As the spring constant is increased at constant volume fraction and coefficient of restitution, it might be expected that the period of an interaction will decrease to zero proportional to

$(m/k)^{1/2}$, and at some (large) value of the spring constant the period of an interaction will become small compared to the time between interactions. Beyond this value, the system will be in a binary contact regime, and the value Z_0 will tend to 1, while all other Z_n for $n \geq 1$ will go to 0. Thus, it is expected that Z_0 will increase continuously to 1 as the spring constant is increased, while Z_n for $n \geq 1$ will decrease to 0. These trends are observed at all angles of inclination $\theta \geq 22^\circ$, indicating that the system can be well described by the binary contact approximation. These trends are not observed at the lowest angle of inclination of 21° , as discussed below.

At the lowest angle of inclination of 21° , the fractions of particles with 1 and 2 contacts, Z_1 and Z_2 , do not change much as the spring constant is increased. The fraction of particles with no contacts Z_0 increases as the spring constant is increased, while the fraction of particles with more than two contacts decreases. The fraction of particles with more than two contacts is less than 0.1 for the values of the scaled spring and damping constants corresponding to real particles even when the angle of inclination is 21° for the linear contact model, although an extrapolation of the data in Fig. 27 might lead to a slightly higher fraction. The fraction of particles with one and two contacts is consistently in the range of 0.2–0.3 for 21° , but they decrease as the angle of inclination is increased. This could indicate that the spring constants studied here are not large enough for the hard particle approximation to be valid, and it is necessary to go to still higher values of the spring constant to attain the hard particle limit. However, it is interesting to note that at the lowest angle of inclination of 21° , the fraction of particles with no contacts is 0.4 for the linear model with scaled spring constants corresponding to real particles. Even for the Hertzian contact model, the extrapolation of the data in Fig. 27 indicates that the fraction of particles with no contacts is in the range of 0.3–0.4. This indicates that the dynamics of the system is dominated by the interactions of particles with zero, one, and two contacts at the lowest angle of 21° . Therefore, the binary contact model is not expected to be accurate at the lowest angle of 21° , and it may be necessary to incorporate multiple contacts.

¹S. B. Savage and D. J. Jeffrey, "The stress tensor in a granular flow at high shear rates," *J. Fluid Mech.* **110**, 255 (1981).

²J. T. Jenkins and S. B. Savage, "A theory for the rapid flow of identical, smooth, nearly elastic particles," *J. Fluid Mech.* **130**, 187 (1983).

³C. K. K. Lun, S. B. Savage, D. J. Jeffrey, and N. Chepurnyi, "Kinetic theories for granular flow: Inelastic particles in Couette flow and slightly inelastic particles in a general flow field," *J. Fluid Mech.* **140**, 223 (1984).

⁴J. T. Jenkins and M. W. Richman, "Grad's 13-moment system for a dense gas of inelastic spheres," *Arch. Ration. Mech. Anal.* **87**, 355 (1985).

⁵V. Kumaran, "Temperature of a granular material fluidised by external vibrations," *Phys. Rev. E* **57**, 5660 (1998).

⁶N. Sela, I. Goldhirsch, and S. H. Noskovicz, "Kinetic theoretical study of a simply sheared two dimensional granular gas to Burnett order," *Phys. Fluids* **8**, 2337 (1996).

⁷N. Sela and I. Goldhirsch, "Hydrodynamic equations for rapid flows of smooth inelastic spheres to Burnett order," *J. Fluid Mech.* **361**, 41 (1998).

⁸V. Kumaran, "Constitutive relations and linear stability of a sheared granular flow," *J. Fluid Mech.* **506**, 1 (2004).

⁹V. Kumaran, "The constitutive relations for the granular flow of rough particles, and its application to the flow down an inclined plane," *J. Fluid Mech.* **561**, 1 (2006).

¹⁰L. E. Silbert, D. Ertas, G. S. Grest, T. C. Halsey, D. Levine, and S. J.

Plimpton, "Granular flow down an inclined plane: Bagnold scaling and rheology," *Phys. Rev. E* **64**, 051302 (2001).

¹¹N. Mitarai and H. Nakanishi, "Bagnold scaling, density plateau, and kinetic theory analysis of dense granular flow," *Phys. Rev. Lett.* **94**, 128001 (2005).

¹²K. A. Reddy and V. Kumaran, "The applicability of constitutive relations from kinetic theory for dense granular flows," *Phys. Rev. E* **76**, 061305 (2007).

¹³K. A. Reddy and V. Kumaran, "Structure and dynamics of two dimensional sheared granular flows," *Phys. Rev. E* **79**, 061303 (2009).

¹⁴D. Ertas and T. C. Halsey, "Granular gravitational collapse and chute flow," *Europhys. Lett.* **60**, 931 (2002).

¹⁵G. Lois, A. Lemaitre, and J. M. Carlson, "Emergence of multi-contact interactions in contact dynamics simulations of granular shear flows," *Europhys. Lett.* **76**, 318 (2006).

¹⁶J. T. Jenkins, "Dense shearing flows of inelastic disks," *Phys. Fluids* **18**, 103307 (2006).

¹⁷J. T. Jenkins, "Dense inclined flows of inelastic spheres," *Granular Matter* **10**, 47 (2007).

¹⁸J. R. Dorfman and E. G. D. Cohen, "Velocity-correlation functions in two and three dimensions: Low density," *Phys. Rev. A* **6**, 776 (1972).

¹⁹M. H. Ernst, B. Cichocki, J. R. Dorfman, J. Sharma, and H. van Beijeren, "Kinetic theory of nonlinear viscous flow in two and three dimensions," *J. Stat. Phys.* **18**, 237 (1978).

²⁰B. Alder and A. W. Wainwright, "Decay of the velocity autocorrelation function," *Phys. Rev. A* **1**, 18 (1970).

²¹V. Kumaran, "Velocity autocorrelations and the viscosity renormalisation in sheared granular flows," *Phys. Rev. Lett.* **96**, 258002 (2006).

²²V. Kumaran, "Dynamics of a dilute sheared inelastic fluid. I. Hydrodynamic modes and the velocity correlation functions," *Phys. Rev. E* **79**, 011301 (2009).

²³V. Kumaran, "Dynamics of a dilute sheared inelastic fluid. II. The effect of correlations," *Phys. Rev. E* **79**, 011302 (2009).

²⁴A. V. Orpe, V. Kumaran, K. A. Reddy, and A. Kudrolli, "Fast decay of the velocity autocorrelation function in dense shear flow of inelastic hard spheres," *Europhys. Lett.* **84**, 64003 (2008).

²⁵T. P. Majmudar and R. P. Behringer, "Contact force measurements and stress-induced anisotropy in granular materials," *Nature (London)* **435**, 1079 (2005).

²⁶A. Ferguson and B. Chakraborty, "Stress and large-scale spatial structures in dense, driven granular flows," *Phys. Rev. E* **73**, 011303 (2006).

²⁷O. Baran, D. Ertas, T. C. Halsey, G. S. Grest, and J. B. Lechman, "Velocity correlations in dense gravity-driven granular chute flow," *Phys. Rev. E* **74**, 051302 (2006).

²⁸V. Kumaran, "Dynamics of dense sheared granular flows. Part 1: Structure and diffusion," *J. Fluid Mech.* **632**, 109 (2009).

²⁹V. Kumaran, "Dynamics of dense sheared granular flows. Part 2: The relative velocity distribution," *J. Fluid Mech.* **632**, 145 (2009).

³⁰M. Babic, H. H. Shen, and H. T. Shen, "The stress tensor in granular shear flows of uniform, deformable disks at high solids concentrations," *J. Fluid Mech.* **219**, 81 (1990).

³¹C. S. Campbell, "Granular shear flows at the elastic limit," *J. Fluid Mech.* **465**, 261 (2002).

³²C. S. Campbell, "Stress-controlled elastic granular shear flows," *J. Fluid Mech.* **539**, 273 (2005).

³³S. Torquato, "Nearest neighbour statistics for packings of hard disks and spheres," *Phys. Rev. E* **51**, 3170 (1995).

³⁴C. Song, P. Wang, and H. Makse, "A phase diagram for jammed matter," *Nature (London)* **453**, 629 (2008).

³⁵K. Shundyak, M. van Hecke, and W. van Saarloos, "Force mobilization and generalized isostaticity in jammed packings of frictional grains," *Phys. Rev. E* **75**, 010301(R) (2007).

³⁶R. J. Bathurst and L. Rothenburg, "Micromechanical aspects of isotropic granular assemblies with linear contact interactions," *Trans. ASME, J. Appl. Mech.* **55**, 17 (1988).

³⁷L. E. Silbert, G. S. Grest, R. E. Brewster, and A. J. Levine, "Rheology and contact lifetimes in dense granular flows," *Phys. Rev. Lett.* **99**, 068002 (2007).

³⁸R. Brewster, L. E. Silbert, G. S. Grest, and A. J. Levine, "Relationship between interparticle contact lifetimes and rheology in gravity-driven granular flows," *Phys. Rev. E* **77**, 061302 (2008).

³⁹L. Brendel, T. Unger, and D. Wolf, in *The Physics of Granular Media*, edited by H. Hinrichsen and D. Wolf (Wiley-VCH, Weinheim, 2005).

- ⁴⁰G. Lois, A. Lematre, and J. M. Carlson, "Numerical tests of constitutive laws for dense granular flows," *Phys. Rev. E* **72**, 051303 (2005).
- ⁴¹G. Lois, A. Lemaitre, and J. M. Carlson, "Spatial force correlations in granular shear flow. I. Numerical evidence," *Phys. Rev. E* **76**, 021302 (2007).
- ⁴²G. Lois, A. Lemaitre, and J. M. Carlson, "Spatial force correlations in granular shear flow. II. Theoretical implications," *Phys. Rev. E* **76**, 021303 (2007).
- ⁴³A. S. Argon, "Plastic deformation in metallic glasses," *Acta Metall.* **27**, 47 (1979).
- ⁴⁴J. S. Langer, "Dynamics of shear-transformation zones in amorphous plasticity: Formulation in terms of an effective disorder temperature," *Phys. Rev. E* **70**, 041502 (2004).
- ⁴⁵V. Kumaran, "Kinetic theory for the density plateau in the granular flow down an inclined plane," *Europhys. Lett.* **73**, 232 (2006).
- ⁴⁶V. Kumaran, "Dense granular flow down an inclined plane—From kinetic theory to granular dynamics," *J. Fluid Mech.* **599**, 120 (2008).
- ⁴⁷C. S. Campbell, "Granular material flows—An overview," *Powder Technol.* **162**, 208 (2006).
- ⁴⁸R. D. Mindlin and H. Deresiewicz, "Elastic spheres in contact under varying oblique forces," *ASME Trans. J. Appl. Mech.* **20**, 327 (1953).
- ⁴⁹*Tables of Physical and Chemical Constants*, edited by G. W. C. Kaye and T. H. Laby (Macmillan, London, 1992).
- ⁵⁰D. M. Cole and J. F. Peters, "A physically based approach to granular media mechanics: Grain-scale experiments, initial results and implications to numerical modeling," *Granular Matter* **9**, 309 (2007).
- ⁵¹*Handbook of Glass Data*, edited by O. V. Mazurin, M. V. Streltsina, and T. P. Shvaiko-Shvaikovskaya (Elsevier, New York, 1993).
- ⁵²D. M. Cole and J. F. Peters, "Grain-scale mechanics of geologic materials and lunar simulants under normal loading," *Granular Matter* **10**, 171 (2008).
- ⁵³P. J. Steinhardt, D. R. Nelson, and M. Ronchetti, "Bond-orientational order in liquids and glasses," *Phys. Rev. B* **28**, 784 (1983).
- ⁵⁴GDR MiDi, "On dense granular flows," *Eur. Phys. J. E* **14**, 341 (2004).
- ⁵⁵B. Bernu and R. Mazighi, "One-dimensional bounce of inelastically colliding marbles on a wall," *J. Phys. A* **23**, 5745 (1990).
- ⁵⁶S. McNamara and W. R. Young, "Inelastic collapse and clumping in a one-dimensional granular medium," *Phys. Fluids A* **4**, 496 (1992).
- ⁵⁷S. McNamara and W. R. Young, "Inelastic collapse in two dimensions," *Phys. Rev. E* **50**, R28 (1994).
- ⁵⁸D. Goldman, M. D. Shattuck, C. Bizon, W. D. McCormick, J. B. Swift, and H. L. Swinney, "Absence of inelastic collapse in a realistic three ball model," *Phys. Rev. E* **57**, 4831 (1998).
- ⁵⁹T. Schwager and T. Poschel, "Coefficient of restitution for viscoelastic spheres: The effect of delayed recovery," *Phys. Rev. E* **78**, 051304 (2008).
- ⁶⁰S. Luding, and S. McNamara, "How to handle the inelastic collapse of a dissipative hard-sphere gas with the TC model," *Granular Matter* **1**, 113 (1998).
- ⁶¹V. Senthil Kumar and V. Kumaran, "Voronoi cell volume distribution and configurational entropy of hard spheres," *J. Chem. Phys.* **123**, 114501 (2005).